Chapter 3: Corona textures in granulites - a review of formation mechanisms and implications for the metamorphic evolution of terranes

3.1 Introduction

In the last two decades, evidence has been mounting which suggests that an equilibrium model of metamorphism is not entirely appropriate and that different rates of intergranular diffusion for major and trace components limit the capacity of a rock to attain equilibrium on both micro- and macro-scales (Carlson, 2002; White et al., 2008). A more realistic model of partial equilibrium, i.e., equilibrium for some components and not for others, is likely to be attained in a rock. In a sense partial equilibrium is fortuitous, since disequilibrium textures preserved in a rock reveal basic physico-chemical reaction dynamics operating during metamorphism that are obscured if a rock equilibrates completely. However, partial disequilibrium also compromises petrographic and geothermobarometric evidence as records of the metamorphic evolution of a terrane and can lead to erroneous interpretations. An understanding of how partial equilibrium manifests petrographically and chemically is, thus, critical in refining our appreciation of metamorphic rocks.

The critical kinetic constraints determining whether full or partial equilibration is attained include: the rate of supply of matter through intergranular diffusion; the rate of reactant dissolution and product nucleation during recrystallisation (interface control); and the rate of supply or removal of heat (Fisher, 1977; Joesten, 1977; Brady, 1983; Tracey and McLellan, 1985; Carlson, 2002). Interface reaction rate, in turn, depends on the affinity for reaction, i.e., the difference between the chemical potentials of diffusing components and their equilibrium values (Carlson, 2002). The slower of these rate-limiting processes determines the nature and extent of reaction and equilibration. During stages of reaction at high temperatures in the presence of a melt or fluid phase, reaction rates are typically interface- rather than diffusion-controlled since diffusion coefficients are large and, thus, unlikely to be rate-limiting. With cooling or loss of the melt or fluid phase, diffusion rates become more important, as does heat flux out of the system. Lower diffusion rates impede chemical communication of requisite components to reaction sites. The bulk rock

composition is effectively partitioned into local compositional domains in local equilibrium with gradients in chemical potential between them.

The most obvious manifestation texturally of diffusion-controlled reaction is the spatial segregation of reaction products in layered corona bands arranged in order of increasing or decreasing chemical potential (Fisher, 1977; Joesten, 1977). Changing pressure and temperature induces reaction between contiguous metastable reactants. With incipient reaction, variable intergranular diffusivities of major components manifest as different length-scales of diffusion, such that the corona domain is partitioned into a continuum of compositional subdomains, or incipient "effective bulk compositions", in which local equilibrium is attained, each with unique chemical potentials. A layered corona assemblage develops, across which transient chemical potential gradients exist, which drive diffusion through the layers. With prolonged reaction or enhanced intergranular diffusion, component flux through the corona layers equalises chemical potentials at all points in the corona. Local incipient bulk compositions of subdomains gradually expand with mass transfer across layers and approach the final steady-state effective bulk composition for the corona as a whole. Equilibrium is attained when no chemical potential gradients exist for any components, despite the spatial segregation of corona phases in layers.

The interpretation of corona textures has traditionally been a primary diagnostic tool for inferring metamorphic *P-T-t* paths and, hence, tectonics (Whitney and McLelland, 1973; Grew, 1980; Joesten, 1986; Droop, 1989; Clarke et al., 1989; Ashworth et al., 1992; White and Clarke, 1997; Norlander et al., 2002; White et al., 2002; Kelsey et al., 2003b; Johnson et al., 2004; Tsunogae and Van Reenen, 2006; Zulbati and Harley, 2007; Hollis et al., 2006). Kinetically constrained conditions may arise on both the prograde and retrograde path but, typically, coronas are thought to have formed during retrogression from peak *P-T* conditions as univariant, or at least very low variance, equilibria are crossed. The topology of the inferred univariants with respect to the peak assemblage has commonly been used to constrain a retrograde *P-T* path (Harley, 1989). Retarded reaction progress under retrograde conditions owing to sluggish reaction kinetics manifests as incomplete reaction between peak phases to produce layered, finely crystalline, spatially segregated reaction products, which armour the peak phases from further reaction.

The inherent assumption of disequilibrium between reactants and corona products has been elegantly questioned recently in a study by White et al. (2002) on metapelites from the Musgrave Block in Australia. Phase equilibria modelling employing pseudosections in KFMASHTO demonstrated that corona textures could realistically be developed in a peak, high variance, assemblage that remains in equilibrium but undergoes large changes in mineral modes as the *P-T* path tracks through the phase field. Thus, it may not be necessary to invoke crossing of univariants and disequilibrium to explain corona textures. Indeed, the amount of decompression required to generate the equilibrium reaction texture described by White et al. (2002) was comparatively minor and may well have been overestimated by earlier workers (Harley, 1989).

While there is a general understanding of processes inducing corona formation (e.g., Harley, 1989; White et al., 2002; Johnson et al., 2004; White et al., 2008), the mechanism for corona development is poorly known since the final steady-state configuration of corona layers observed in a rock reflects the complex evolution of chemical potential relationships with changing temperature, pressure, and bulk composition. These same complexities must also govern metamorphic processes on the prograde path at larger scales. However, greater melt or fluid volumes and higher temperatures on the prograde path facilitate equalization of chemical potentials through accelerated diffusion in the assemblage, such that only the spatial sequestration of phases (for example, between melt-rich leucosomes and melt-poor mesosomes) attests to the compositional partitioning of the rock and attendant chemical potential gradients that must have prevailed during diffusion-controlled reaction (White et al., 2004). In coronas, disequilibrium is frozen in the rock, preserving incipient reaction textures. They are, therefore, the best petrographic evidence available to us to allow the study of the evolution of chemical potential gradients governing the reorganization of components within a rock with changing *P-T-X* conditions (e.g., White et al., 2008). Furthermore, the small, manageable volumes of coronas make them logistically easier to study (reaction band thicknesses vary from a few microns up to millimetres in thickness) and, since reactant minerals are retained adjacent to the corona bands, the effective equilibrium bulk compositions are also reasonably easy to constrain.

Two distinct paradigms of corona growth have evolved in the last four decades, namely, synchronous, *single-stage,* steady-state (e.g., Ashworth and Sheplev, 1997) and *sequential* (Joesten 1986; White and Clarke, 1997) diffusion-controlled, growth of multilayered coronas.

3.2 Single-stage, steady-state, diffusion-controlled corona growth (SSDC)

The single-stage, steady-state multilayer growth model attributes corona development to diffusion-controlled reaction mechanisms at constant pressure and temperature, with local equilibrium and chemical potential gradients across each layer and the corona as a whole (Figure 3.1). The spatial segregation of phases into layers reflects relative mobility of components owing to variable intergranular diffusivities rather than distinct *P-T* conditions. All layers in the reaction bands coexist contemporaneously with infinitesimal thickness at the incipient stages of reaction. Only layer thickness increases with reaction duration and no change to the internal structure of the corona occurs. Chemical potential gradients evolve toward a steady-state and constant final configuration balancing the rate of production and consumption of each component within each layer (Korzhinskii, 1959; Joesten, 1977; Mongkoltip and Ashworth, 1983; Foster, 1986; Grant, 1988; Johnson and Carlson 1990; Carlson and Johnson, 1991; Ashworth and Birdi, 1990; Ashworth et al., 1992; Ashworth and Sheplev, 1997; Markl et al., 1998; Ashworth et al., 1998).

Figure 3.1 demonstrates incipient stages of SSDC corona formation chemographically and in chemical potential space. Consider two phases (A and D) initially at equilibrium under P_1 and T_1 with bulk composition indicated by the orange circle (Figure 3.1a). New P and T conditions (P_2, T_2) are kinetically inhibited and reaction progress becomes diffusion-controlled. Relative differences in intergranular diffusivities partition the original bulk composition (orange circle) into two endmember, non-overlapping, local bulk compositions, typically an alumina-poor bulk composition (blue square) contrasting with an alumina-rich composition (yellow triangle) intermediate between the reactant compositions (Figure 3.1b). The product mineral assemblage layers are spatially segregated in local equilibrium and comprise the mineral assemblage stabilised in each local effective bulk composition,

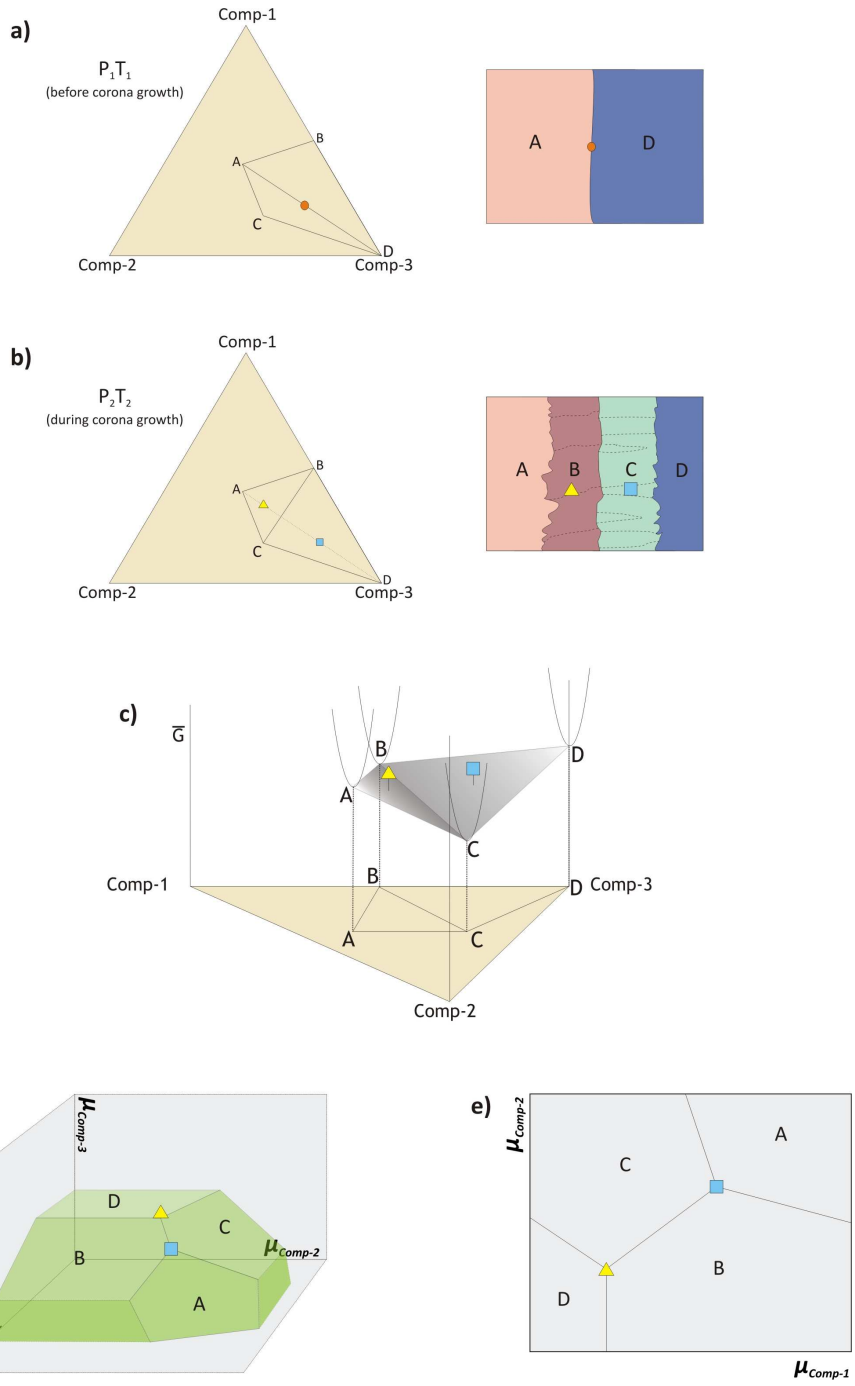

Figure 3.1: Chemographic relationships and chemical potential saturation surfaces for local transient equilibria at corona boundaries during incipient stages of SSDC corona growth (modified after Joesten, 1977). (a) Original phases (A and D) initially at equilibrium under P_1 and T_1 with bulk composition indicated by the orange circle. (b) New P and T conditions (P_2, T_2) are kinetically inhibited and reaction progress becomes diffusion-controlled. The corona domain is partitioned into a continuum of compositional subdomains, or incipient "effective bulk compositions", in which local equilibrium is attained, each with unique chemical potentials. (c) Ternary G-X surface, in which local equilibria are separated by chemical potential differences. (d) The chemical potential saturation surface for each of the local phase assemblages. (e) Projection of the saturation surface on the μ_{comp1}-μ_{comp2} plane. Chemical potential gradients between local equilibria drive diffusion of components from one compositional domain to another until chemical potentials are equalised and equilibrium is attained.

i.e., the local bulk composition indicated by the blue square stabilises assemblage BCD and, similarly, the bulk composition indicated by the yellow triangle stabilises assemblage ABC (Figure 3.1b). A ternary *G-X* surface indicates that the tangent planes to the minimum free energy assemblages have different orientations and, accordingly, components have different chemical potentials in each assemblage (Figure 3.1c). The coexistence of two local juxtaposed equilibria buffers the chemical potentials of diffusing components across the coronas (Joesten, 1977). Figure 3.1d represents the associated, isothermal-isobaric chemical potential saturation surface for each of the local phase assemblages (modified after Joesten, 1977). Each local bulk composition, represented by a three-phase assemblage, is invariant in chemical potential space at constant pressure and temperature. The invariant assemblage ABC (local bulk composition yellow triangle) lies at a higher chemical potential for component 3 and lower chemical potentials for components 1 and 2, than does the invariant assemblage BCD represented by the blue square. A projection of the saturation surface on the μ_{comp1}-μ_{comp2} plane (Figure 3.1e) more clearly indicates the difference between chemical potentials for each local equilibrium. Maintenance of these local equilibria requires that chemical potential gradients must exist across each layer and the system as a whole is in disequilibrium, which drives diffusion of components from one compositional domain to another. Chemical potential differences across each layer adjust to steady-state values that balance the rates of production and consumption of each component within the layer (Joesten, 1977). Chemical potential gradients for rapidly diffusing components may be eliminated across the corona, whilst those for the slowest moving components are maintained, establishing partial equilibrium.

Continued corona evolution entails the growth of a layer assemblage at the expense of its neighbour by reaction with the diffusing components (Joesten, 1977). The relative diffusive fluxes of components in adjacent layers determine which mineral phases are consumed and produced at each layer boundary, as well as the reaction stoichiometry (Joesten, 1977; Fisher, 1977). All mineral layers grow at the same time, by a set of diffusion-controlled reactions at layer contacts which liberate and consume components in the appropriate proportions to account for mass balance in the overall system (Joesten, 1977, 1986; Fisher, 1977). The only layer that grows at both contacts is the layer which initially contained the original reactant interface

(Joesten, 1977; Joesten, 1986). Fisher (1973) demonstrated that diffusion will automatically tend to shift potentials toward values such that the flux differences at every point in a structure balance local reactions, thereby establishing a steady-state configuration. Growth of coronas will slow and eventually cease when diffusion paths become too tortuous and long; chemical potential gradients approach values too low to drive significant diffusion; and/or as intergranular diffusivities are reduced with cooling during retrogression (Joesten, 1977; Fisher, 1977; Ashworth and Sheplev, 1997).

Figure 3.2 demonstrates a natural example of the single-stage, steady-state, diffusion-controlled growth of corona layers at constant *P* and *T*. The corona in Figure 3.2 is a schematic reconstruction of those described by Johnson and Carlson (1990) from metagabbros in the Adirondack Mountains. In Figure 3.2a, the primary igneous assemblage includes contiguous olivine and plagioclase. During later granulite facies metamorphism, primary olivine and plagioclase are no longer stable, and are replaced by a new stable assemblage including orthopyroxene, clinopyroxene, plagioclase and garnet. Rates of *P-T* change exceed rates of intergranular diffusion in the dry mafic bulk composition and diffusion-controlled reaction ensues. Variable relative rates of intergranular diffusion manifest as spatially segregated product layers depending on the diffusion range of each component. The corona domain is partitioned into a continuum of compositional subdomains or incipient effective bulk compositions in which local equilibrium is attained, each with unique chemical potentials. Since Al is the slowest-diffusing component, the most aluminous product phase adjoins the most aluminous reactant and asymmetric composition profiles for slower-diffusing species are established across product bands, e.g., Al content in product bands increases toward the Al-rich reactant. Fe, Mg and Si released from olivine diffuse down chemical potential gradients toward plagioclase, whereas Na, Ca, Al and Si released from plagioclase diffuse toward olivine. Reactions occur at layer boundaries and layers expand as diffusion progresses (Figure 3.2b). The width and composition of each corona layer depend on the relative fluxes of the diffusing elements. The product mineral assemblage does not change as reaction proceeds. Chemical potentials and fluxes approach steady-state values. Mg, Ca, Na and Al are imported into the corona and Fe and Si are exported from the corona. Minor spinel clouding occurs in reactant

plagioclase as Ca and Si diffuse preferentially into the reaction band, creating a Si deficiency that stabilises spinel in relict reactant plagioclase (Johnson and Carlson, 1990).

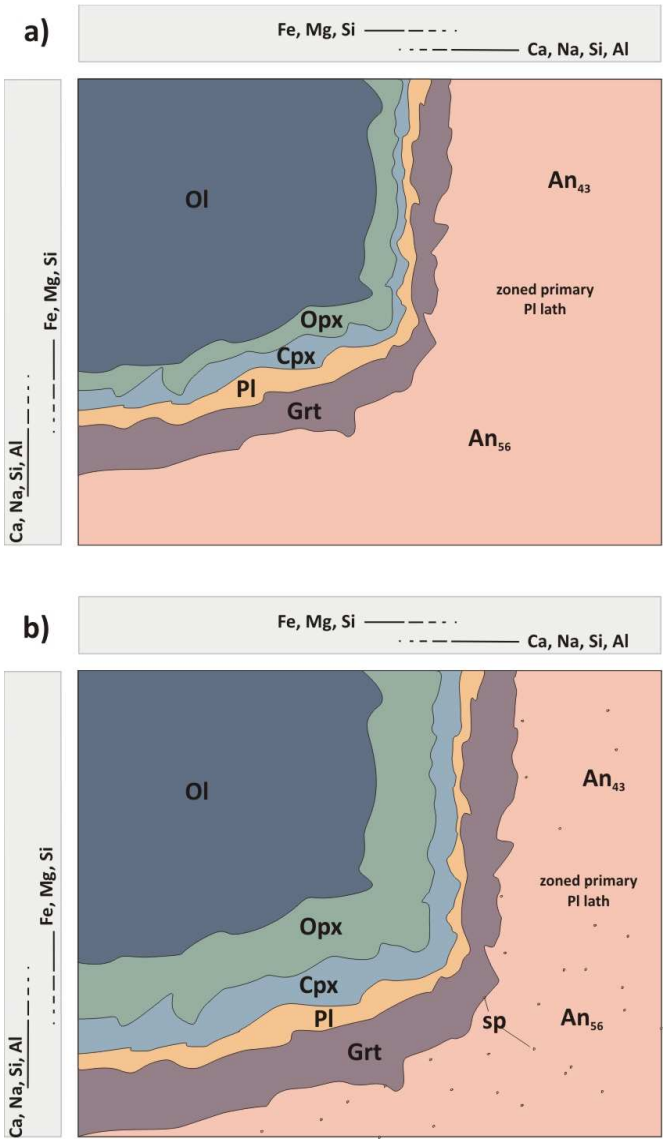

Figure 3.2: Open-system, single-stage, steady-state, diffusion-controlled growth of prograde corona layers between olivine and plagioclase (modified after Johnson and Carlson, 1990). (a) With incipient reaction, different rates of intergranular diffusion for major components manifest as spatially segregated layers. The corona domain is partitioned into a continuum of compositional subdomains or incipient effective bulk compositions in which local equilibrium is attained, each with unique chemical potentials. Fe, Mg and Si released from olivine diffuse down chemical potential gradients toward plagioclase, whereas Na, Ca, Al and Si released from plagioclase diffuse toward olivine. Layers comprising the slowest diffusing species (Al) adjoin the most aluminous reactant. (b) Reactions occur at layer boundaries and layers expand as diffusion progresses. The width and composition of each corona layer depend on the relative fluxes of the diffusing elements. Minor spinel clouding occurs in reactant plagioclase as Ca and Si diffuse preferentially into the reaction band, creating a Si deficiency in reactant plagioclase.

3.3 Sequential diffusion-controlled corona growth (SEQ)

The sequential, diffusion-controlled corona layer growth model involves successive, step-wise growth of layers, overprinting and partial re-equilibration of younger corona layers as new equilibria are encountered on either the prograde or retrograde path, typically with changing pressure and/or temperature but also through changing component fluxes through the corona as a function of evolving local effective bulk compositions (hereafter referred to as EBC) (e.g., Griffin, 1972; Griffin and Heier, 1973; Joesten, 1986; Droop, 1989; Indares, 1993; Johnson et al., 2004; White et al., 2002). In contrast to the SSDC model, the internal layer configuration of the corona reaction band evolves with time as new layers develop and old layers are resorbed. Relative diffusion fluxes and attendant chemical potential differences shift and evolve from one steady-state configuration to another under new *P-T-X* conditions.

Sequential corona development with changing pressure and temperature has been demonstrated in prograde coronas in mafic rocks between olivine and plagioclase by Griffin (1972). He derived a sequential model for corona formation that involved cooling from igneous temperatures at 8 - 11 kbar and crossing of univariant equilibria (Figure 3.3a-e). A schematic *P-T* grid is included in Figure 3.3f to elucidate reaction progress. Initially, olivine and plagioclase crystallized at point (A) in the grid. As the rock cooled, it was buried and followed the path delineated by the red arrow. At point B (Figure 3.3a), igneous olivine and plagioclase reacted to produce Tschermakitic clinopyroxene (Cpx I) and aluminous orthopyroxene (Opx I). As the rock tracked through *P-T* space from B to C (Figure 3.3b), the clinopyroxene (Cpx I) exsolved spinel and anorthite to form a less Tschermakitic clinopyroxene (Cpx II). This clinopyroxene was partly consumed at point C (Figure 3.3c) to produce garnet and a jadeitic clinopyroxene (Cpx III). Further cooling into the eclogite facies produced omphacitic clinopyroxene and garnet with lesser quartz at point D (Figure 3.3d). Finally, decompression on exhumation induced the exsolution of the jadeite component from omphacite to yield diopside (Cpx IV) and plagioclase towards point E (Figure 3.3e). Mork (1986) also invoked a sequential model for corona formation between olivine and plagioclase in western Norway, however, he proposed a clockwise metamorphic *P-T* path rather than single-stage cooling from igneous temperatures.

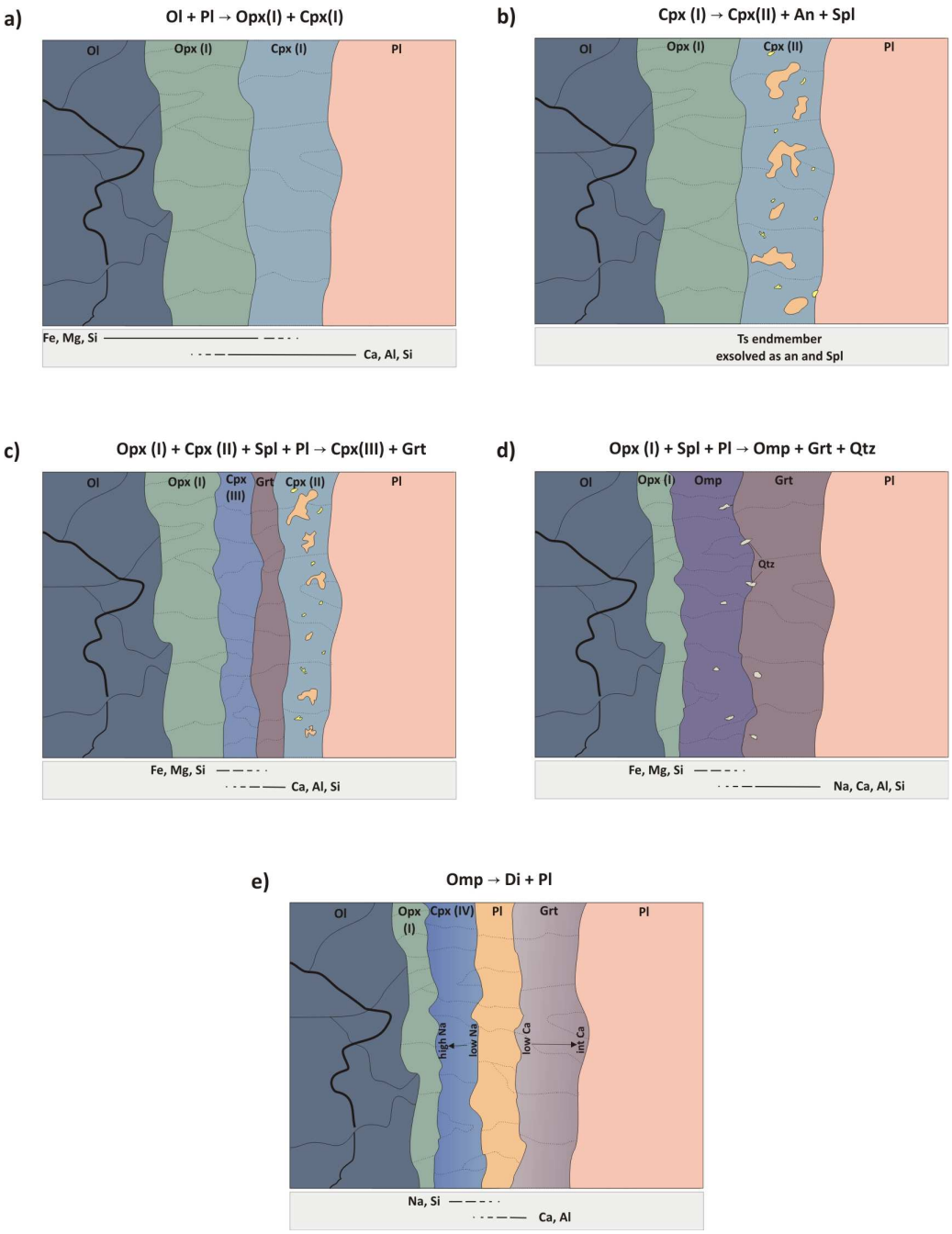

Figure 3.3: Sequential layer development in a corona between olivine and plagioclase after Griffin (1972). During cooling from igneous temperatures at 8 - 11 kbar, discrete layers developed in response to changes in pressure and temperature as univariant equilibria were crossed on the P-T path, and older layers were overprinted to produce stable intervening layers. (a) The original stable olivine and plagioclase assemblage reacts to form orthopyroxene and clinopyroxene. (b) Clinopyroxene breaks down to form a less Tschermakitic composition with plagioclase and spinel. (c) With progressive cooling, this clinopyroxene reacts with orthopyroxene, spinel and plagioclase to produce garnet. (d) Orthopyroxene reacts with spinel and plagioclase to produce omphacite, garnet and quartz. (e) Omphacite decomposes to clinopyroxene and plagioclase.

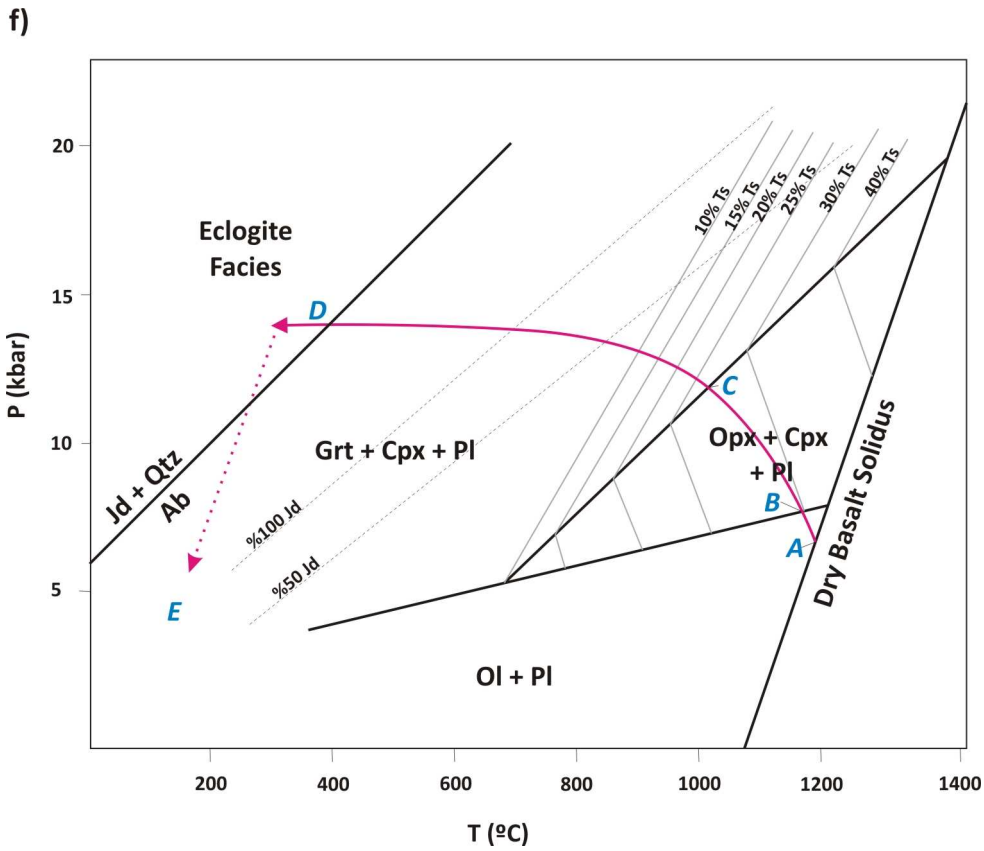

Figure 3.3 continued: Sequential layer development in a corona between olivine and plagioclase after Griffin (1972). (f) Schematic P-T grid indicating relevant univariant equilibria crossed along the P-T path, inducing the sequence of reactions required for layer development.

Sequential corona development may occur at constant pressure and temperature with changing component fluxes across the corona band. A multilayer corona may evolve in a steady or quasi-stationary state controlled by diffusion (SSDC) and then subsequently modify through back-reaction between two adjacent layers at constant pressure and temperature through changing composition of the effective equilibration volume as the composition of a reactant evolves with protracted reaction. Brady (1977) and Vidale (1969) introduced a modification to the steady-state model that was first used to explain corona variability by Johnson and Carlson (1990). Vidale (1969) modelled the development of calc-silicate bands in a system with waning availability of certain components. According to his model, rapidly diffusing components in a reaction band will eventually eliminate their chemical potential gradients. The chemical potentials of those rapidly diffusing components are then determined by equilibria outside of the corona band. As the number of components exerting a diffusive control on the reaction is reduced by one, so one

mineral phase is lost from the band (Vidale, 1969, Brady, 1977). This manifests as 'cannibalisation' of corona layers comprising the rapidly diffusing components. The original steady state is modified as the system enters a transient state that will evolve through time toward a new steady state with constant chemical potential gradients.

Johnson and Carlson (1990) demonstrated the sequential development of corona layers with changing component fluxes through the corona (Figure 3.4). As the reactant plagioclase is gradually exhausted in Ca and Si, it is converted from labradorite to andesine + spinel (Figure 3.4a). The product mineral assemblage evolves into a new transient state in response to reduced Ca and Si availability. The chemical potentials of Ca and Si are determined by equilibria outside of the corona band. Initially Ca, and then Si, chemical potentials become dictated by external equilibria in which their availability wanes. This manifests as the destabilisation and subsequent 'cannibalisation' of first the plagioclase corona layer and then clinopyroxene (Figure 3.4a, b) as the system evolves toward a new steady-state scenario with constant chemical potential gradients. Johnson and Carlson (1990) employed this model to explain variability in the corona product assemblages developed between plagioclase and olivine in the Adirondack Mountains. Initially, all corona bands were plagioclase and clinopyroxene-bearing, but evolved to different final configurations with greater or lesser cannibalisation of these phases, depending on the availability of Ca and Si in the surrounding phases. Where the olivine grain adjoins the spinel-poor plagioclase (originally less calcic, An_{43}), both product plagioclase and clinopyroxene have been consumed, and the orthopyroxene is in contact with garnet. In contrast, where olivine is adjacent to spinel-rich reactant plagioclase (originally more calcic, An_{56}), corona plagioclase and clinopyroxene are retained (Figure 3.4c).

Sequential layer development in a corona through variation of *P*, *T* and changing bulk composition of the corona reaction volume is invoked by Indares (1993) to explain coronas between olivine and plagioclase in an olivine gabbro from the Shabogamo Intrusive Suite, Eastern Grenville Province. Initially, at high *P* and *T*, under eclogite facies conditions, calcic plagioclase reacts with olivine to form orthopyroxene and garnet coronas (Figure 3.5a). The relative difference in

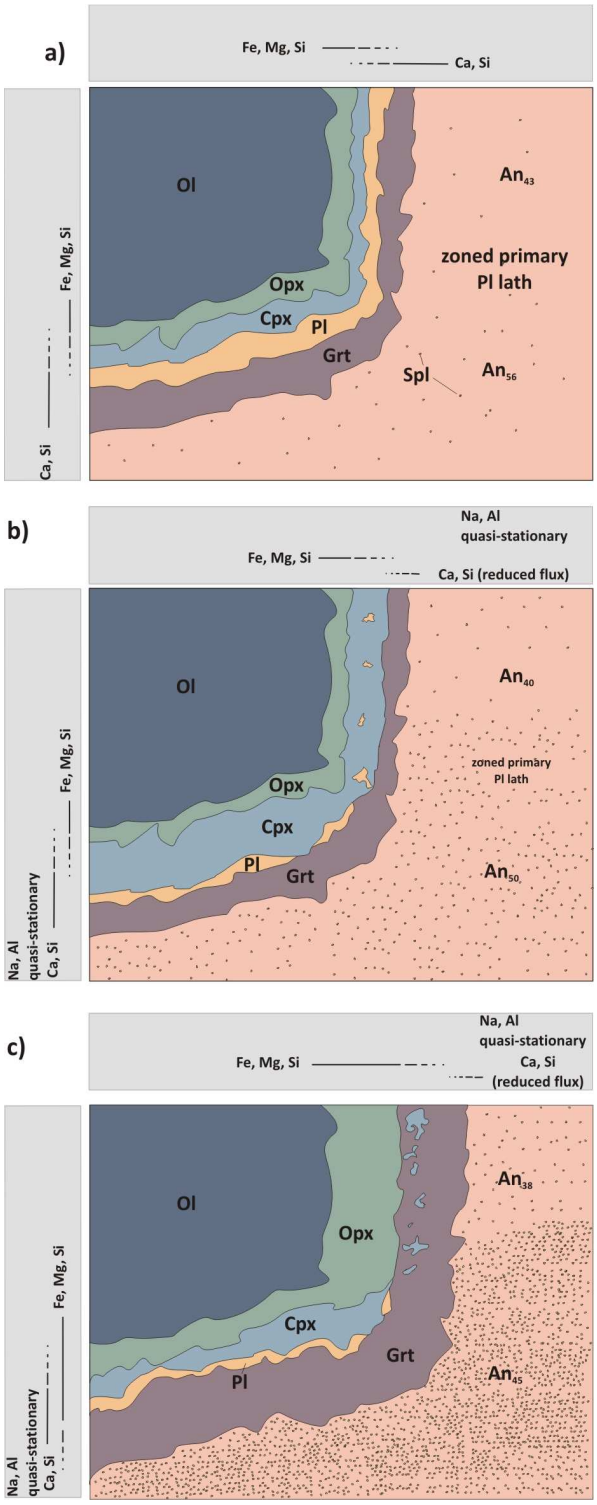

Figure 3.4: Sequential model of corona layer growth at constant P and T (modified after Johnson and Carlson, 1990), accommodating waning boundary fluxes of rapidly diffusing components from the reactants into the corona in an open system. (a) Initial steady-state layer configuration for an olivine-plagioclase corona. (b) Depletion of Ca and Si in the reactants leads to the consumption of plagioclase and then (c) clinopyroxene in transient states. The system will gradually evolve toward a new steady state. Cannibalisation of corona plagioclase and clinopyroxene is more enhanced where the original reactant is Ca-poor (top-right, An_{38}).

intergranular diffusivities of components manifests as two distinct corona layers over which chemical potential gradients exist, grading from aluminous garnet adjacent to plagioclase to Al-poor orthopyroxene adjacent to olivine. Excess Al in the plagioclase is accommodated by the formation of corundum (Figure 3.5a). At the same pressure and temperature, the garnet layer grows by reaction between calcic plagioclase and corona orthopyroxene in a local effective bulk composition different from that which produced the initial corona orthopyroxene and garnet, which included olivine (Figure 3.5b). Continued reaction generates excess Si and Al in the reactant plagioclase, which reacts with corundum to form kyanite (Figure 3.5b). In Figure 3.5c, the reactant plagioclase is relatively enriched in Na through the two former reactions. Na now diffuses out of plagioclase and reacts with corona orthopyroxene and garnet to form omphacite. In response, more kyanite forms in the plagioclase to accommodate excess residual Si and Al. With subsequent exhumation and decompression, corona garnet reacts with kyanite and corundum in plagioclase to form spinel and more calcic plagioclase (Figure 3.5d). In addition, garnet reacts with omphacite and some excess Si to produce intervening plagioclase.

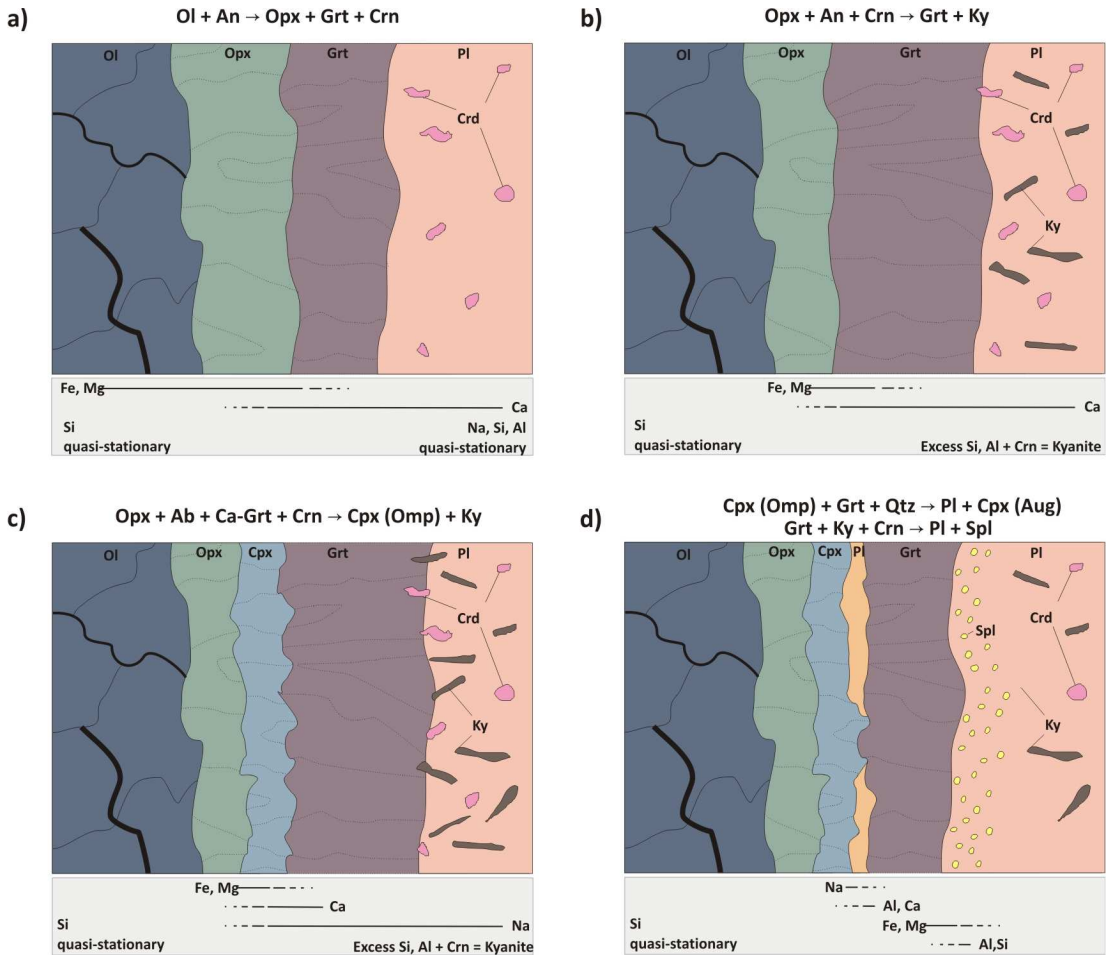

Figure 3.5: Sequential model of corona layer growth between plagioclase and olivine through varying component fluxes across the corona bands and later due to decompression (modified after Indares, 1993). Corona layer growth in (a)-(c) occurs under constant high P and T, from discrete reactions between reactants initially and then subsequently between individual corona layers as component fluxes vary across the corona. The formation of the plagioclase layer in (d) is ascribed to decompression. Detailed reaction mechanisms are discussed in the text.

3.4 Determining a sequential or single-stage model of corona growth?

Determining which model of corona formation is applicable in a specific context is commonly difficult but very important if information on the *P-T* path is to be gleaned correctly from the corona (White and Clarke, 1997). This is critically evident in contrasting interpretations of the coronas formed between olivine and plagioclase in metagabbros from Risor, Norway (Joesten, 1986; Ashworth, 1986). Two elegant arguments are crafted by these authors in support of the sequential layer growth model and single-stage, steady-state, diffusion-controlled layer growth model, respectively.

Joesten (1986) cites textural evidence and the diffusional instability of any closed system steady-state diffusion model for the coronas in support of a primary magmatic origin for the coronas followed by secondary annealing. Joesten (1986) suggested that cuspate olivine-orthopyroxene contacts; thickening of orthopyroxene layers at narrow terminations of olivine grains; irregular contacts between orthopyroxene-spinel and amphibole-spinel layers; and sectoral heterogeneity in the corona assemblage depending on the adjacent magmatic phase (i.e., either plagioclase, amphibole or clinopyroxene), are all inconsistent with a diffusion-controlled origin. He suggested these features were more likely a result of olivine dissolution in a melt, followed by the sequential growth of corona layers with cooling at magmatic temperatures above the olivine-plagioclase stability field. Joesten (1986) proposed that these primary magmatic coronas were diffusionally unstable and that they were spontaneously partially to completely annealed on cooling.

In contrast, Ashworth (1986) suggested the Risor coronas formed by the single-stage, steady-state, diffusion-controlled replacement of plagioclase and olivine with an open-system modification to mass-balance model constraints. Textural evidence apparently inconsistent with a diffusion model was attributed to locally variable kinetic controls on reaction mechanism, e.g., epitaxial growth of tabular amphibole on magmatic grains vs. heterogeneous nucleation at reactant contacts. Ashworth (1986) did not address the sectoral heterogeneity of the coronas nor the irregular contacts between amphibole-spinel and orthopyroxene-spinel layers; however, it is conceivable that variation in the bulk composition of the equilibration volume - both

spatially and temporally as reaction proceeded - may account for such heterogeneity (e.g., Johnson and Carlson 1990).

Alternative sequential models of corona formation, invoking varying pressure, temperature and/or boundary fluxes may similarly have important implications for reconstruction of *P-T* paths. For the same corona textures between olivine and plagioclase, three different *P-T* paths were constructed by Griffin (1972), Johnson and Carlson (1990) and Indares (1993), reflecting three disparate mechanisms for sequential corona formation, namely, changing pressure and temperature (Griffin, 1972; Joesten, 1986), changing component fluxes (Johnson and Carlson, 1990), or a combination of all three parameters (Indares, 1993). Mass-balance constraints and compositional zonation within each corona assemblage were cited in each case in support of the adopted model.

Criteria for the identification of single-stage, steady-state layer growth include: mineral zonation and a marked spatial organization of product reaction bands such that each layer represents a 'non-overlapping volume in compositional space' (Joesten, 1977; Fisher, 1977), all arranged in an orderly sequence of increasing or decreasing chemical potential (Fisher, 1977). If the corona has not attained equilibrium, asymmetric composition profiles in minerals within a corona layer and the corona as a whole are consistent with chemical potential gradients induced by relative differences in intergranular diffusion rates of components at approximately constant *P-T* conditions (Indares, 1993, White and Clarke, 1997). Symmetric, radial zoning of phases with respect to grain boundaries is consistent with a sequential corona formation model. Mass balance constraints commonly preclude the formation of an intervening layer by reaction between two initially contiguous layers and this evidence most convincingly negates the sequential layer growth model or provides resolution as to a mechanism of sequential layer growth. Even so, evidence may be equivocal and it may not be possible to exclusively establish single-stage, diffusion-controlled multilayer corona growth from step-wise, sequential growth in response to changing *P-T* conditions or component fluxes. In these cases, tectonic context and structural data might provide independent constraints favouring one model over the other.

3.5 Controls on corona development in pelitic and mafic granulites

A comprehensive review of coronas described in the literature from metamafic and metapelitic rocks is included in Tables 3.1 and 3.2. Table 3.1 details coronas formed on the prograde path, and Table 3.2 lists a selection of the more numerous occurrences of coronas formed during retrograde re-equilibration. Selected coronas from mafic and pelitic rocks are schematically illustrated in Figures 3.6 and 3.7, respectively. Corona assemblages and microstructure in both metapelites and metamafic rocks vary considerably depending on (a) metamorphic conditions (*P*, *T* and aH_2O), (b) formation mechanism through either steady-state or sequential layer development, (c) reactant compositions, (d) diffusion kinetics, and (e) the amount of deformation or strain intensity on either the prograde or retrograde path.

3.5.1 Pressure, temperature and aH_2O

Pressure, temperature and aH_2O conditions determine which mineral phases manifest in the corona. In olivine gabbros or troctolites from the Adirondacks, New York, coronal assemblages vary from *Ol* | Opx+Cpx | Grt | *Pl* (reactants in italics) in the Adirondack Highlands (Johnson and Carlson, 1990 - Figure 3.6a) to *Ol* | Opx | Cpx+Spl | *Pl* in the southwest (Whitney and McLelland, 1973 - Figure 3.6b). The presence of garnet in the former case is attributed to higher pressures compared to the southwest. In the Newer Basic Intrusion of NE Scotland, the coronal assemblage *Ol* | Opx | Hbl+Spl | *Pl* is observed (Mongkoltip and Ashworth, 1983 - Figure 3.6c). In this case, Hbl is favoured over Cpx under higher aH_2O conditions. Similarly, the dominance of hornblende in the corona assemblage between garnet and clinopyroxene in Carlson and Johnson (1991) (Figure 3.6d) vs. the restriction of pargasite to the layer closet to garnet in Baldwin et al. (2004) (Figure 3.6e), is attributed to higher aH_2O in the former corona compositional domain. In metapelites, coronas after sapphirine and quartz comprise the sequence *Spr* | Sil | Opx | *Qtz* at higher pressures, but *Spr* | Sil | Opx+Crd | *Qtz* at lower pressures and temperatures and/or higher aH_2O conditions (e.g., Lal et al., 1987). Coronas after gedrite and kyanite from the Thor Odin Dome in British Columbia comprise the sequence *Ged* | Crd | Crd+Spl sympl | Crd+Crn sympl | *Ky* (Norlander

et al., 2002 - Figure 3.7a). The lower-temperature equivalent corona (assuming minimal bulk compositional differences) is *Ky* | St | Crd | *Ged* in metapelites from Errabiddy granulites in Western Australia (Baker et al., 1987).

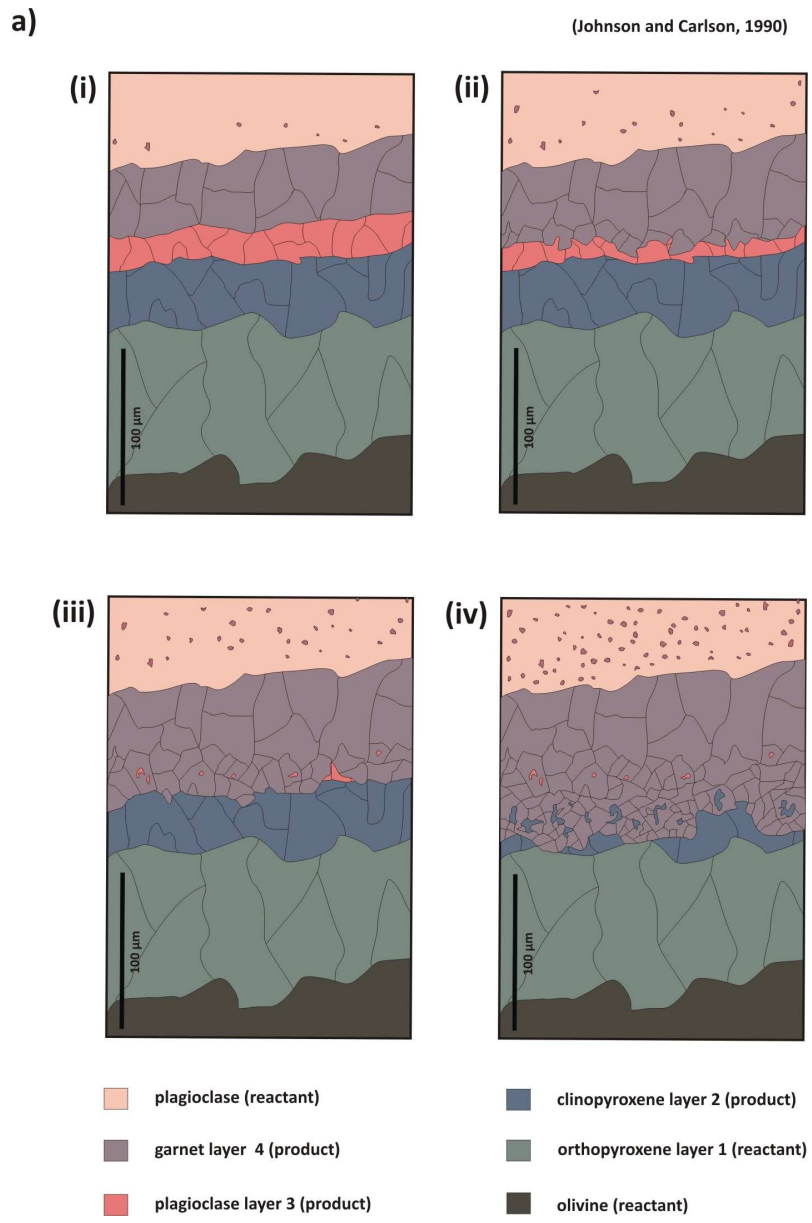

Figure 3.6: Common corona textures developed in mafic granulites. (a) Common prograde complex coronas between olivine and plagioclase from the Adirondack Highlands (after Johnson and Carlson, 1990) demonstrating the range of corona layer configurations observed, which reflects progressive Si and Ca depletion in the reactant plagioclase: (i) Incipient corona with both plagioclase and clinopyroxene stable. (ii) Waning Ca and Si fluxes from reactant Pl induce cannibalisation of first (ii) plagioclase then (iii) clinopyroxene. (iv) The most evolved corona configuration is where garnet encroaches upon orthopyroxene. Spinel clouding in plagioclase reflects progressive Si depletion in the reactant. There is no variation in the product phase compositions across the corona, implying complete equilibration.

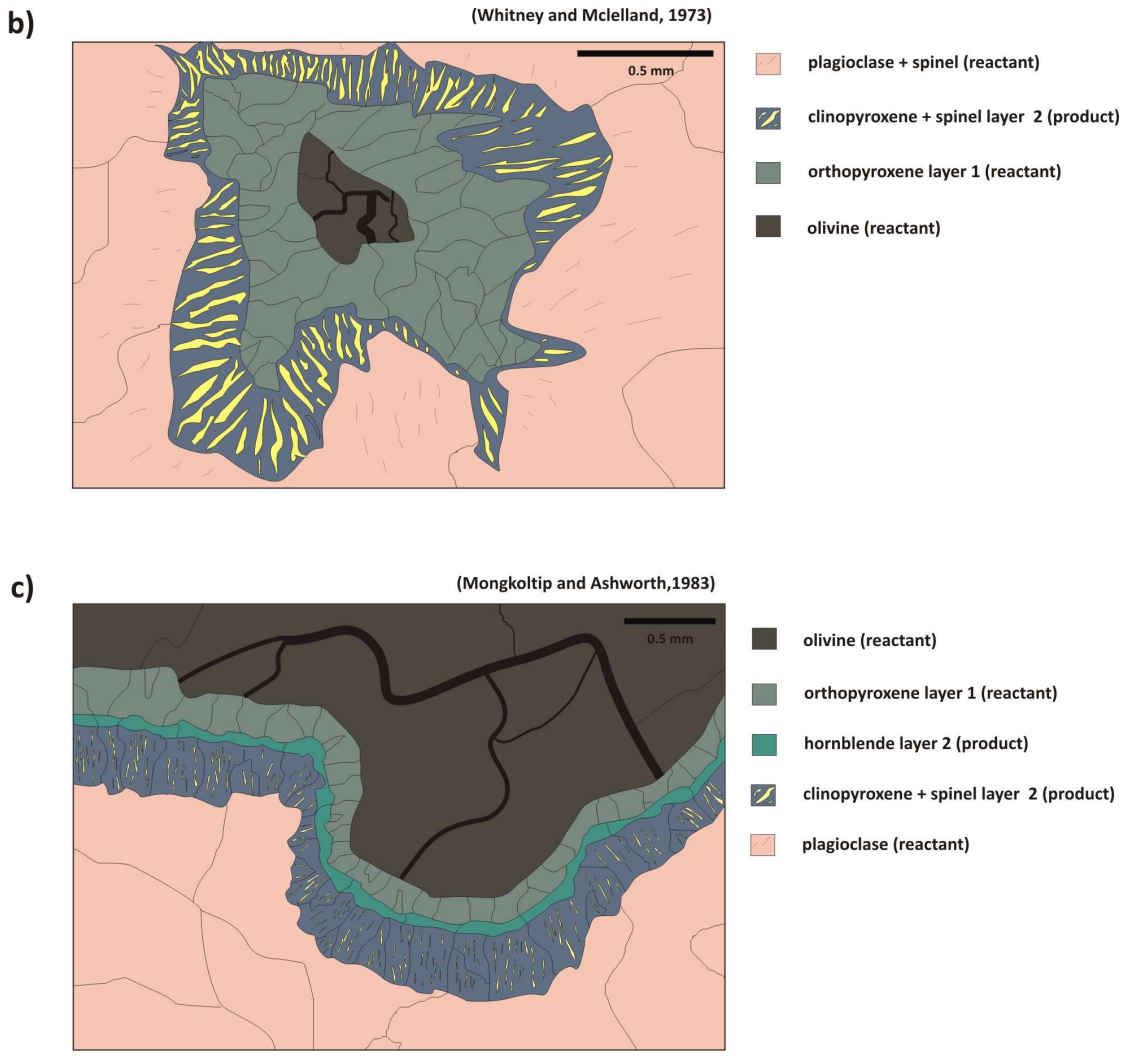

Figure 3.6 continued: Common corona textures developed in mafic granulites. (b) Prograde corona developed between olivine and plagioclase during burial following shallow intrusion in the southwestern Adirondacks, New York (after Whitney and McLelland, 1973). Garnet is not present in this corona owing to low inferred pressures during corona reaction. There is no variation in X_{Mg} of pyroxenes. (c) A retrograde corona developed between olivine and plagioclase in an olivine metagabbro from northeast Scotland (after Mongkoltip and Ashworth, 1983). The presence of amphibole suggests higher aH_2O than in more anhydrous domainal compositions where only clinopyroxene is stable. Al content and X_{Fe} of Opx and Hbl increase toward Pl reactant. Details in Tables 3.1 and 3.2.

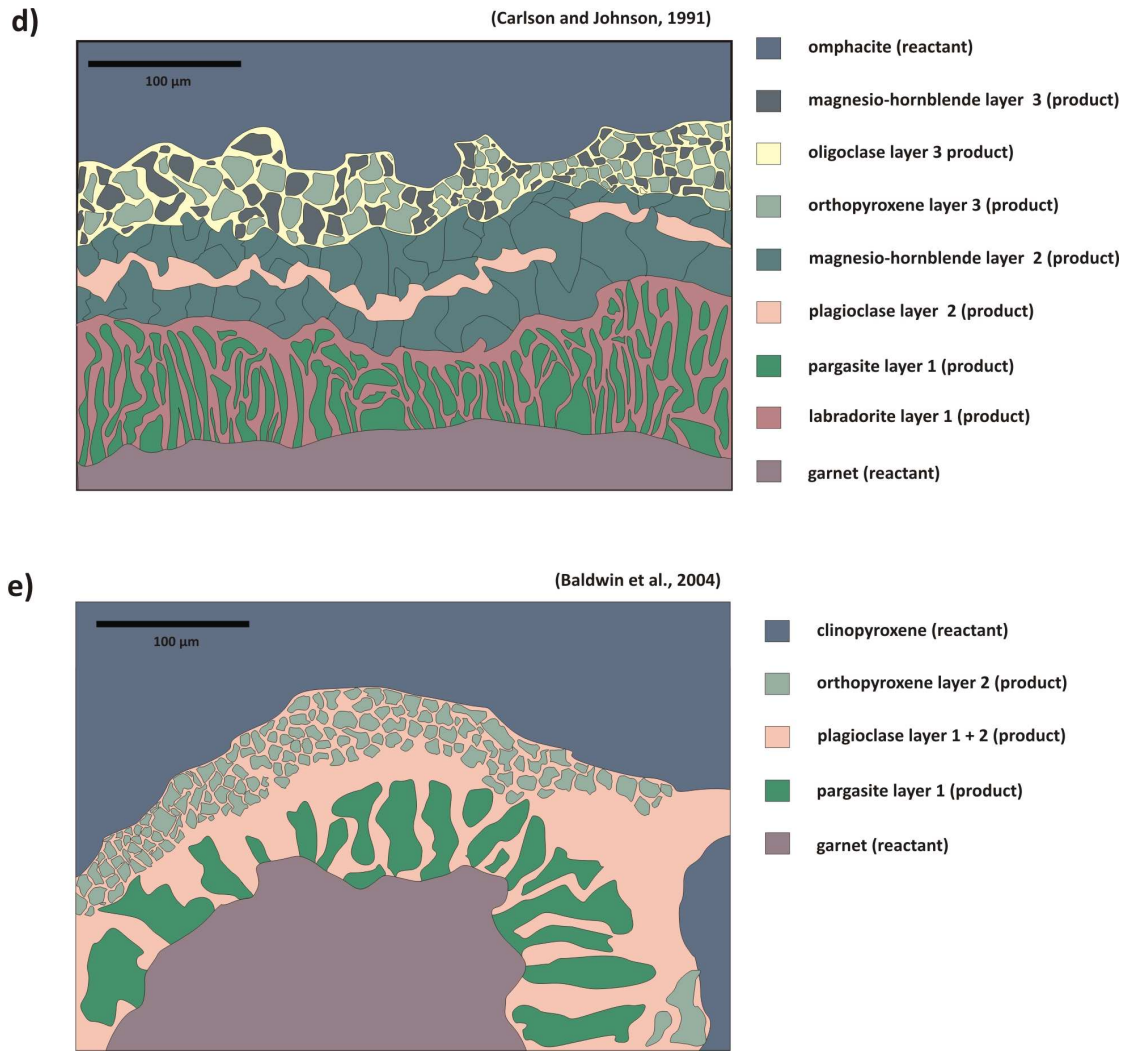

Figure 3.6 continued: Common corona textures developed in mafic granulites. d) Retrograde corona developed between garnet and clinopyroxene during a static thermal event with the intrusion of numerous granite plutons in the Llano Uplift, Texas (after Carlson and Johnson, 1991). The presence of hornblende implies relatively high aH_2O during reaction. Both hornblende and plagioclase are asymmetrically zoned across the corona band. Plagioclase becomes less calcic (An_{35} to An_{18}) and amphibole Fe/Mg and Al/Si ratios decrease toward omphacite. (e) Retrograde corona developed between garnet and clinopyroxene from the Snowbird Tectonic Zone, Western Canadian Shield (after Baldwin et al., 2004). The restricted distribution of hornblende in this corona compared to that in (d), suggests a less hydrous bulk corona composition. Marked zonation in plagioclase occurs from An_{91} adjacent garnet to An_{44} at clinopyroxene margin. Details in Tables 3.1 and 3.2.

3.5.2 Reaction mechanism: single-stage vs. sequential development

Corona assemblages are also governed by the mechanism by which they formed, i.e., either in a single-stage, steady-state event, or as sequential layers in response to varying pressure, temperature or component fluxes into the reaction volume. Johnson and Carlson (1990) characterised a range of corona textures between olivine and plagioclase in the Adirondacks, New York (Figures 3.4 and 3.6a) and attributed different corona configurations to varying extents of internal corona cannibalisation with waning Ca and Si fluxes across the corona depending on the original composition of the plagioclase reactant. Alternatively, intervening layers may develop with cooling as length-scales of diffusion become more constrained and the corona compositional domain partitions into smaller-volume local equilibria in which a secondary corona assemblage may develop by reaction between two contiguous layers at new *P* and *T* conditions (e.g., Griffin, 1972; Brandt et al., 2003).

3.5.3 Reactant compositions

The compositions of local reactants principally determine the effective bulk composition of the corona, with a minor degree of open-system communication with matrix beyond the immediate reactants. The most obvious manifestation of local compositional control on corona configuration is demonstrated by the three main types of coronas observed in mafic rocks, where metasomatic exchange with the enclosing rock is minimal and the corona bulk composition is principally determined by the reactants. Local corona bulk compositions comprising orthopyroxene, clinopyroxene, plagioclase and garnet form after olivine and plagioclase (*Ol* │ Opx │ Cpx │ Pl │ Grt │ *Pl* - Figure 3.6a). More aluminous, hydrous corona bulk compositions stabilise amphibole, plagioclase and orthopyroxene after garnet, clinopyroxene and externally derived H_2O-rich fluid (*Grt* │ Prg │ Pl │ Cpx/Opx │ *Cpx* - Figure 3.6d, e). Commonly, orthopyroxene reacts with plagioclase to yield clinopyroxene, quartz and garnet coronas (*Cpx* │ Cpx/Opx │ Qtz │ Grt │ *Pl* - Figure 3.6f, g).

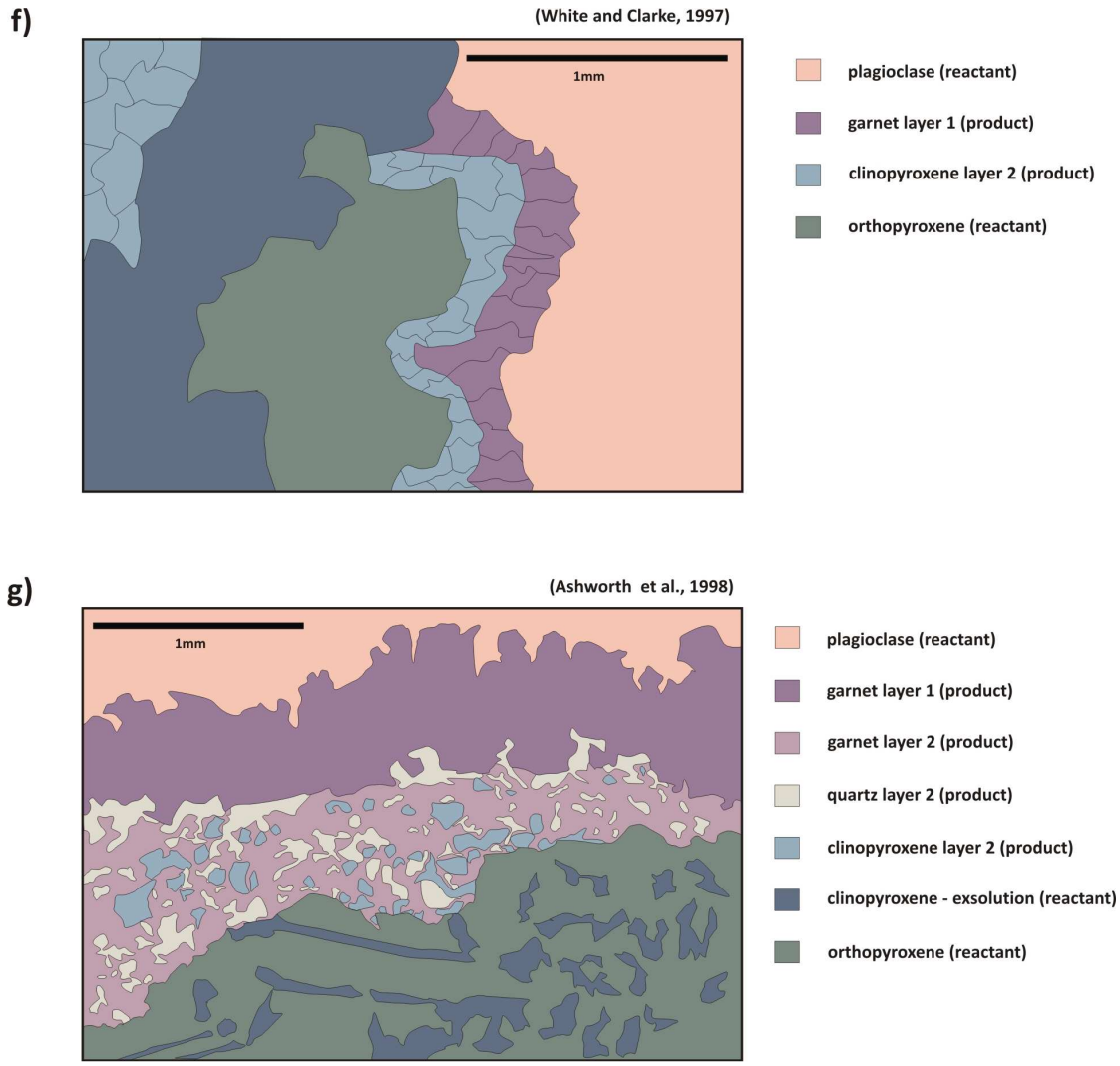

Figure 3.6 continued: Common corona textures developed in mafic granulites. (f) Prograde corona developed between plagioclase and orthopyroxene during deformation-enhanced reaction in a dolerite towards a shear zone (after White and Clarke, 1997). Garnet exhibits asymmetric zonation as X_{Alm}, X_{Prp} and X_{Grs} increase toward Pl. Garnet zoning diminishes toward shear zone. (g) Prograde corona developed between plagioclase and orthopyroxene in a mafic granulite from Yenisey Ridge, Siberia (after Ashworth et al., 1998). Layer 1 garnet is zoned: Fe increases and Ca decreases (X_{Grs}: 0.24 - 0.21; X_{Alm}: 0.54 - 0.60) toward layer 2. A slight compositional perturbation four-fifths of the distance across layer 1 is thought to mark the initial Pl/Opx boundary. In layers 3 and 4, Ca in garnet is almost constant, with higher Fe and lower Mg than in layer 1. No systematic zonation is observed in pyroxene. Non-equilibrium thermobarometric estimates for corona formation are 740 ± 20 °C and 9.5 ± 0.7 kbar (Ashworth et al., 2001). Details in Tables 3.1 and 3.2.

Markl et al. (1998) described coronas after fayalite and K-feldspar or plagioclase (*Fa* | Opx | Grt+Opx | *Pl/Kfs*), in which the layer thicknesses, product proportions and their compositions vary systematically depending on whether plagioclase or K-feldspar is the reactant. Carlson and Johnson (1991) described a corona after garnet and quartz comprising the layer sequence *Grt* | Pl+Mgt | Opx+Aug | *Qtz* in a metagabbro from the Llano Uplift in Texas. In metapelites, coronas after garnet and quartz typically yield a coronal assemblage of *Grt* | Crd+Opx | ±Pl | Opx | *Qtz* (Hollis et al., 2006 - Figure 3.7b). The presence of augite, plagioclase and magnetite in the metagabbro may be attributed to significantly more calcic garnet (~8 wt% CaO) with a higher X_{Fe} than typical pelitic garnets. Van Lamoen (1979) and Nishiyama (1983) reviewed reported coronas after olivine and plagioclase in metamafic rocks and conclusively demonstrated a correlation between the composition of reactant olivine and product orthopyroxene.

Sectoral development in complex coronas is perhaps the most obvious manifestation of reactant compostional control on corona mineralogy and morphology. Kelsey et al. (2003b) described sectoral development of coronas around garnet in pelitic granulites from Mather paragneiss in the Rauer Group, Antarctica (Figure 3.7c). In these granulites, garnet is enclosed by a complex corona which comprises *Grt* | Crd+Opx symp | Opx | *Qtz* where garnet was initially adjacent to quartz and *Grt* | Crd+Opx symp | Pl | *Bt*, where initially adjacent to biotite. These corona sectors appear to define unique effective bulk compositions. The sharp changes in mineral proportions between sectors attests to the limited degree of chemical communication between the Grt-Bt and Grt-Qtz compositional domains. Bruno et al. (2001) described coronas after biotite and quartz or feldspar, in which corona mineralogy varies around a single biotite grain from *Bt* | Grt | *Qtz* where biotite abuts quartz, to *Bt* | Grt | Grt+Qtz | Phg+Qtz | *Kfs* where biotite is adjacent to K-feldspar and *Bt* | Grt | Grt+Jd | *Pl* where plagioclase encloses biotite (Figure 3.7d).

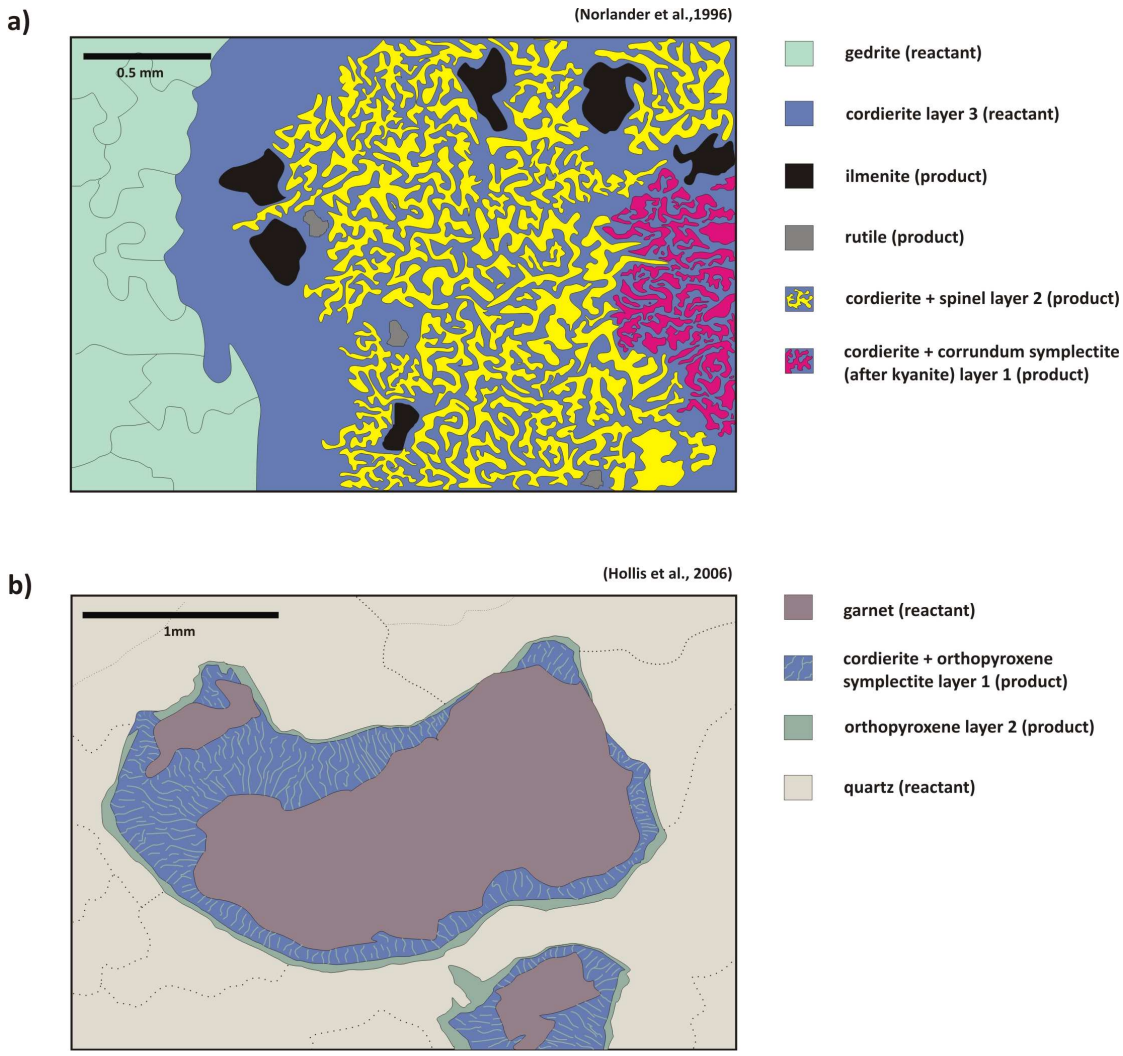

Figure 3.7: Common corona textures developed in pelitic granulites. (a) Complex corona between kyanite and gedrite (after Norlander et al., 1996). No compositional variation in any corona phases was observed. Conditions of formation constrained at < 5 kbar and ~ 750 °C with TWQ and conventional thermobarometers. (b) Common complex corona developed after garnet and quartz (after Hollis et al., 2006). No systematic variation is described in corona products. Details in Tables 3.1 and 3.2.

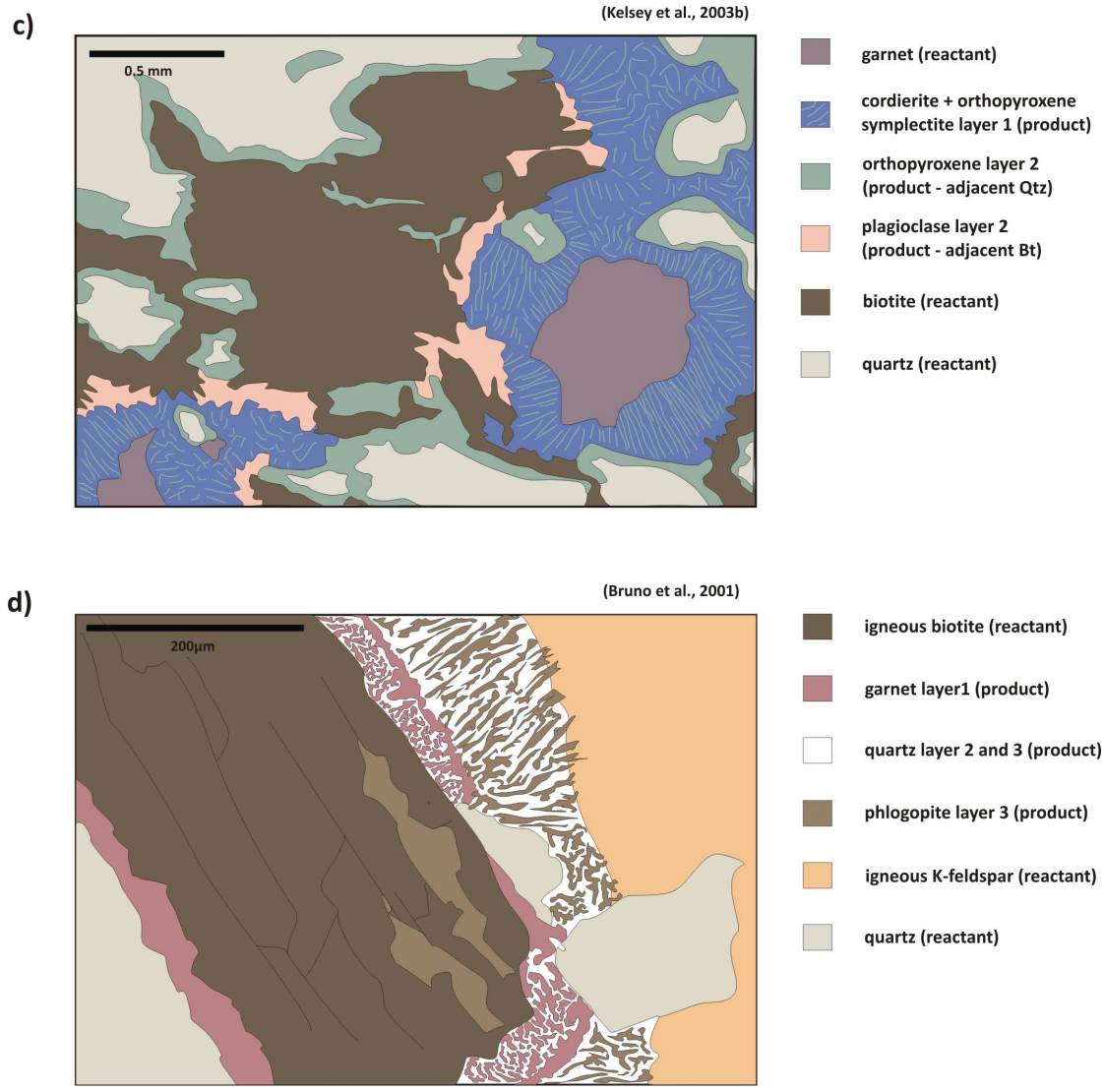

Figure 3.7 continued: Common corona textures developed in pelitic granulites. (c) Complex sectoral corona between garnet, biotite and quartz. Monomineralic plagioclase is constrained to the corona immediately adjacent to biotite. Similarly, blocky orthopyroxene occurs only in the corona sectors where garnet reacts with quartz (after Kelsey et al., 2003b). Cordierite X_{Mg} varies across symplectite increasing toward orthopyroxene in general. No variation in orthopyroxene composition is observed. (d) Symplectite-dominated corona developed between biotite and K-feldspar (after Bruno et al., 2001). Where biotite reacts with quartz, monomineralic garnet comprises the corona. Elsewhere, a complex, symplectite-dominated corona comprising garnet, quartz and phlogopite occurs where biotite and feldspar react. Corona garnet is weakly zoned. Details in Tables 3.1 and 3.2.

3.5.4 Diffusion kinetics

The spatial array of corona product bands and the presence or absence of associated symplectite is a function of diffusion kinetics, i.e., relative intergranular diffusivities of major system components. Typically, Al and Si are relatively immobile compared to more rapidly diffusing components such as Fe, Mg and, to a lesser extent, Ca (e.g., Johnson and Carlson, 1990; Carlson and Johnson, 1991; Ashworth and Birdi, 1990; Ashworth et al., 1992; Ashworth and Sheplev, 1997). In natural coronas that have formed in a single-stage, steady-state, diffusion-controlled scenario, typically limited Al diffusion manifests as both modal and phase compositional zonation in the corona, i.e., Al-rich minerals occur in layers closest to the aluminous reactant and, within these layers, the corona minerals exhibit asymmetric zonation in compositional profiles, e.g., *y*(Opx) increases toward the Al-rich reactant. Since Fe and Mg typically diffuse more rapidly than Al, ferromagnesian minerals tend to segregate into layers farthest from the aluminous reactant. X_{Fe} varies across the corona depending on relative intergranular diffusivities of Fe and Mg. Coronas after sapphirine and quartz (Ellis et al., 1980 - Figure 3.7e) and between sillimanite and orthopyroxene (Kriegsman et al., 1999 - Figure 3.7f) demonstrate spatial segregation of aluminous corona layers (sillimanite and sapphirine, respectively) from more Fe- and Mg-rich corona products (orthopyroxene and cordierite, respectively) in metapelites. Coronas after garnet and clinopyroxene in more mafic bulk compositions segregate into pargasite adjacent to garnet and orthopyroxene+plagioclase adjacent to clinopyroxene (Baldwin et al., 2004 - Figure 3.6e).

Kinetically-constrained reaction rates arise most commonly on the retrograde *P-T* path (Table 3.2) in melt-depleted, restitic bulk rock compositions. In metapelites, coronal reaction textures are frequently attributed to isothermal decompression following peak conditions on a clockwise *P-T* path (e.g., coronas after garnet and quartz; Kelsey et al., 2003b - Figure 3.7c) or to isobaric cooling (e.g., coronas after sapphirine and quartz; Grew, 1980 - Figure 3.7e). White et al. (2002), however, urge caution in inferring large amounts of decompression and cooling along the retrograde path to produce corona textures; phase equilibria modelling of spinel-bearing symplectites after garnet from an Fe-rich pelitic granulite in the Musgrave

Block, Australia, suggests coronas might develop on any number of retrograde *P-T* path trajectories through a high-variance field in which the mode of garnet is decreasing while that of the corona products is increasing (Figure 3.7g). Large amounts of decompression are, thus, not required to produce symplectites after garnet and estimates of decompression from other terranes may well have been overestimated (e.g., Harley, 1989).

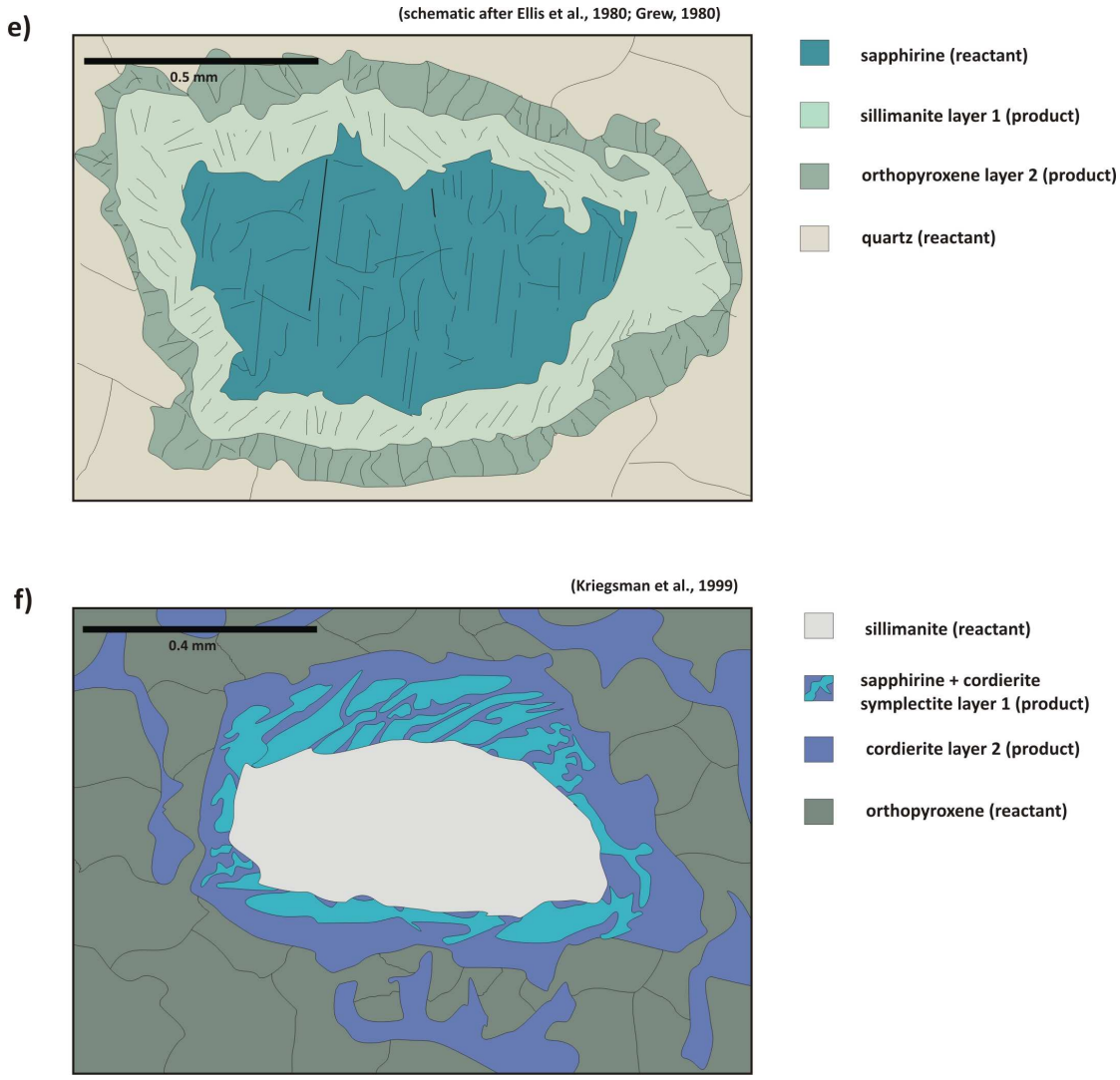

Figure 3.7 continued: Common corona textures developed in pelitic granulites. (e) Monomineralic sillimanite and orthopyroxene developed after sapphirine and quartz (after Ellis et al., 1980 and Grew, 1980). (f) Retrograde sapphirine-cordierite symplectite and monomineralic cordierite moat developed after orthopyroxene and sillimanite on an isothermal decompressive P-T path (after Kriegsman et al., 1999). Details in Tables 3.1 and 3.2.

Coronas developed on the prograde path are far less common than coronas that form after peak phases during retrogression (Table 3.1 and 3.2), owing largely to more prolonged reaction duration; the presence of a melt or fluid and, hence, greater length-scales of diffusion; and associated deformation on the prograde path. Thus, the kinetically-constrained conditions on the prograde path suitable for corona growth occur in unique tectonic circumstances where: (a) deformation is absent (e.g., White and Clarke, 1997 - Figure 3.6f); (b) at low $a\mathrm{H_2O}$ in mafic rocks (Ashworth et al., 1998 - Figure 3.6g; Johnson and Carlson 1990 - Figure 3.6a) or in melt-depleted pelitic restites and (c) the rate of change of pressure and temperature occurs anomalously quickly such that diffusion rates are exceeded. Typically, the latter scenario arises in rapidly cooling contact aureoles (Johnson et al., 2004 - Figure 3.7h; Mcfarlane et al., 2003; Ings and Owen, 2002; Barboza and Bergantz, 2000; Wheeler et al., 2004; Daczko et al., 2002; Dasgupta et al., 1997; Joesten and Fisher, 1988) but will also be demonstrated for the pelitic granulites in the Vredefort Dome (Chapter 4).

3.5.5 Deformation and strain

High strain intensities have been shown to enhance equilibration (Holyoke and Tullis, 2006). White and Clarke (1997) described coronas developed after orthopyroxene and plagioclase in a dolerite adjacent to a shear zone in the Western Musgrave Block, Australia (Figure 3.6f). As the shear zone is approached, coronas diminish in complexity until complete equilibration and recrystallisation is attained in highest strain domains within the shear zone. Koons et al. (1987) documented similar findings in a quartz diorite from the Sesia Zone, Western Alps. Equilibrium domains progressively approach that of the bulk rock composition with increasing deformation without any change in pressure and temperature. White and Clarke (1997) attributed enhanced equilibration in high-strain domains to a combination of reduction in grain size with attendant increase in intergranular area, accelerated intracrystalline diffusion and nucleation, increased permeability and $a\mathrm{H_2O}$.

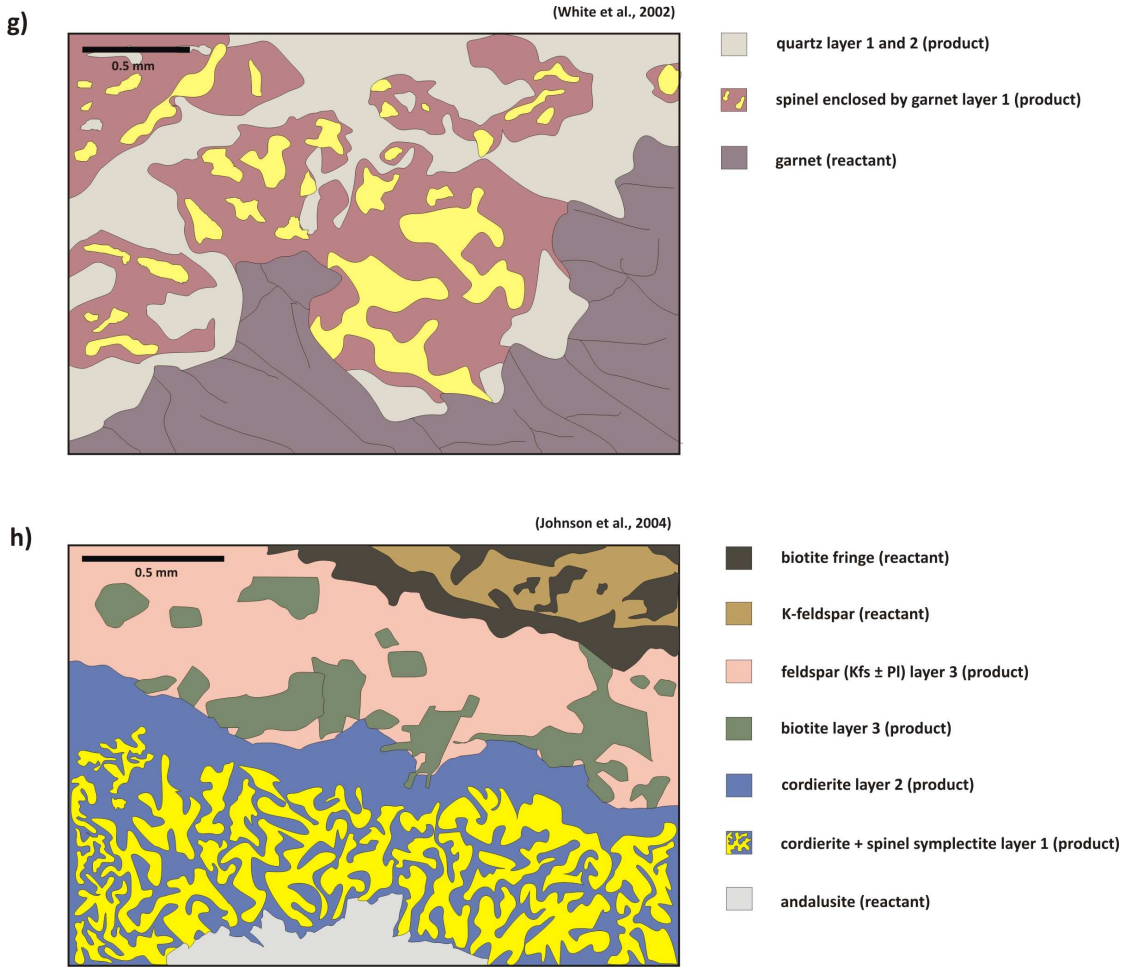

Figure 3.7 continued: Common corona textures developed in pelitic granulites. (g) Retrograde spinel-garnet symplectite replacing peak garnet during post-peak decompression (after White et al., 2002). This corona develops in response to changing modes in a high variance equilibrium assemblage. No univariant reaction is crossed. (h) Prograde complex corona comprising spinel-cordierite symplectite and leucocratic biotite, K-feldspar and plagioclase after andalusite (after Johnson et al., 2004). X_{Mg} of cordierite decreases toward biotite (0.55 - 0.51) with no variation in spinel composition. Cordierite moat formation occurs during an andalusite melting reaction consuming quartz and biotite, followed by continued breakdown of andalusite to cordierite-spinel symplectite in SiO_2 deficient domains. Details in Tables 3.1 and 3.2.

Table 3.1: Summary of prograde corona occurrences in the literature

Tag	Bulk comp	Location	Reactants	Corona product assemblage	Corona Thickness, Vermicule size, Vermicule spacing	Equilibration	*P, T* of corona formation	Inferred *P-T* path	Layer growth model	Diffusion model	Comments
JC90	Olivine metagabbro	Adirondack Mountains, New York	Ol - Pl	*Ol* | Opx | Cpx | Grt | *Pl* *Ol* | Opx+Cpx | Pl | Grt | *Pl*	Corona thickness: *250 µm* Vermicule size: *4 - 50 µm* Vermicule spacing: *8 µm (measured from BSE images)* Vermicule Shape: *Columnar Opx and Grt (cannibalised Pl and Cpx - vermicular)* Orientation: *Columnar grains oriented perpendicular to grain boundaries*	Complete - no variation in composition of corona product phases.	Assuming pressure of 8 kbar, Grt-Cpx (Ellis and Green, 1979) thermometer: Northern Adirondacks: 881 ºC Southern Adirondacks: 708 ºC	IBC, anticlockwise	SSDC - gradual exhaustion of Pl as a reactant	Open: L ratios not constrained tightly	Formation at high pressure and low aH_2O. As Ca is depleted in reactant plagioclase, product plagioclase and clinopyroxene are 'cannibalised'. Geochronological evidence negates a magmatic origin and cooling from igneous temperatures at high pressures as a cause of reaction and, instead, invokes a much younger superimposed metamorphic event (cf. Whitney and McLelland, 1973).
N83	Olivine metagabbro	Mt Ikoma, Osaka, Japan	Ol - Pl	*Ol* | Opx | Hbl+Spl symp | *Pl*	Corona thickness: *50 - 300 µm* *Opx: < 30 µm* *Hbl+Spl: < 60 µm* Vermicule size: -- Vermicule spacing: -- Vermicule Shape: *Hbl - fibrous rods and needles, Spl - vermicular* Orientation: *Vermicules and rods perpendicular to layer boundaries*	Disequilibrium - no systematic variation is observed.	Amphibolite facies - no quantitative thermobarometry	Not specified	SSDC	Closed: L_{ti}/L_{SiSi} >1 and L_{ti}/L_{SiSi} > L_{AlAl}/L_{SiSi}	
J04	Metapelite	Phepane Dome, Bushveld Complex Aureole	And - Bt+matrix	*And* | Crd+Spl symp | Crd | Kfs+Pl+Bt leucosome | *35mol% fringe Bt+15mol% matrix Crd, Kfs, Qtz, Bt*	Corona thickness: *Crd+Spl symp < 1 mm; Crd: < 0.5 mm* Vermicule size: *0.01 - 0.25 mm* Vermicule spacing:-- Vermicule Shape: *Crd - granoblastic-polygonal, Spl - vermicular; vermicules perpendicular to layer boundaries*	Disequilibrium. X_{Mg} of Crd decreases toward Bt (0.55 - 0.51); no variation in spinel composition.	700 - 725 ºC, 3 kbar (*P-T-X* relationships from pseudosection)	Clockwise	SEQ	None	Crd moat formation during And + Bt melting reaction consuming quartz, followed by continued breakdown of And to Crd+Spl symplectite in SiO_2 deficient domains.
WC97	Dolerite	Western Musgrave Block, Australia	*Corona 1:* Opx - Pl *Corona 2:* Cpx - Pl *Corona 3:* Cpx - Pl *Corona 4:* Ilm - Pl	*Corona 1:* *Opx* | Cpx | $\pm Pl_2$ | Grt | *Pl* *Corona 2:* *Cpx_1* | Cpx_2 | Grt | *Pl* *Corona 3:* *Cpx* | Cpx_2 | Hbl | *Pl* *Corona 4:* *Ilm* | Bt | Grt+Bt symp | Grt | *Pl*	Corona thickness: *Corona 1: 0.25 mm* *Corona 2: < 0.5 mm* *Corona 3: < 0.2 mm* Vermicule size: *< 10 - 125 µm* Vermicule spacing:-- Vermicule Shape: *Columnar Opx and subhedral, elongate Grt and Hbl oriented perpendicular to layer boundaries*	No systematic variation in composition of Hbl, Pl (An_{20-25}) and Cpx. Garnet asymmetric zoning: X_{Alm}, X_{Prp} and X_{Grs} increase toward Pl (X_{Grs} = 0.18 - 0.24 to grossular peaks of up to X_{Grs} = 0.4). Grt zoning diminishes toward shear zone.	*T* ~ 750 °C and 12 - 14 kbar (core and rim compositions used in average *P-T* mode in THERMOCALC based on two assemblages: Grt, Pl, Cpx, Qtz and Grt, Pl, Hbl, Qtz	-	Hybrid SSDC	None	Equilibration is enhanced in high strain domains via a reduction in grain size leading to an increase in intergranular area, enhanced intracrystalline diffusion and nucleation, increased permeability and fluid access (White and Clarke, 1997).
I93	Olivine gabbro	Shabogamo Intrusive Suite, Eastern Grenville Province	*Corona 1:* Ol - Pl *Corona 2:* Opx - Pl	*Corona 1:* *Ol* | Opx+Cpx | Pl | Grt | *Pl* *Corona 2:* *Opx* | Cpx | Grt | *Pl*	Corona thickness: *Corona 1: < 1 mm* *Corona 2: < 4 mm* Vermicule size: -- Vermicule spacing:-- Vermicule Shape: *Granoblastic-polygonal with no preferred orientation*	Asymmetrical zonation in Grt (X_{Alm}: 0.4 - 0.58 and X_{Prp}: 0.17 - 0.24) from Pl toward Opx. Layers more calcic in cores. No systematic zoning in Cpx. Opx homogenous.	*T* ~ 700 - 800°C and 16 kbar (core and rim compositions used) by Grt-Cpx-Pl-Qtz thermobarometry	Clockwise with steep ITD	SEQ	-	-
JF88	Chert/calc-silicate nodules in marble	Christmas Mountains, Texas (aureole enclosing alkali gabbro)	Cal - Qtz	*Cal* | Wo | *Qtz* (102 - 125m from gabbro) *Cal* | Tilleyite | Wo | *Qtz* (23 - 15m from gabbro) *Cal* | Spurrite | Wo | *Qtz* (13 - 0m from gabbro)		No compositional variation in corona products possible.	No pressure estimate. Thermal gradient (from numerical models of cooling pluton) ranges from 600 ºC (115m from contact) to 1030 ºC (at contact)	-	SSDC	Closed: L_{CaCa}/L_{SiSi} = 42 and L_{CaCa}/L_{CO2} > 1	Numerical modelling of diffusion controlled mineral growth in the aureole, yielded kinetic coefficients for non-isothermal processes.

Table 3.1 continued: Summary of prograde corona occurrences in the literature

Tag	Bulk comp	Location	Reactants	Corona product assemblage	Corona Thickness, Vermicule size, Vermicule spacing	Equilibration	*P, T* of corona formation	Inferred *P-T* path	Layer growth model	Diffusion model	Comments
ABE92	Basic orthogneiss	Jotun Nappe Complex, Norway	Ol - Pl	*Ol* | Opx/Tlc | Hbl | Hbl+Spl symp | Ep+ Hbl +Spl symp | Ep+Ts+St+Spl symp | Ep+Ts+Ky symp | *Pl*	Corona thickness: *< 160 µm* Vermicule size: *Not resolvable* Vermicule spacing:-- Vermicule Shape: *Granoblastic-polygonal/interlobate epidote, spinel + hornblende needles/rods* Orientation: *Needles weakly oriented perpendicular layer boundaries*	Disequilibrium. Hbl Al/Si ratios decrease toward olivine. No systematic variation in Fe/Mg ratio of Spl and Hbl (ΔAl = 3.13 - 3.74 a.p.f.u; ΔMg = 2.17 - 2.97 a.p.f.u).	Epidote-amphibolite facies. No quantitative thermobarometry	ITD	SSDC	Open: $L_{Fe2+}, L_{Mg} > L_{Fe3+} \geq L_{Ca} > L_{Al} \geq L_{Si}$	St+Ky and Ky+Hbl stable in H_2O-undersaturated conditions
K87	Quartz Diorite	Sesia Zone, Western Alps	Bt - Matrix	*Bt* | Ms | Grt | *Matrix (Jd+Qtz+Zo)*	Corona thickness: *100 µm* Vermicule size: *< 50 µm* Vermicule spacing:-- Vermicule Shape: *Granoblastic-polygonal*	Disequilibrium. X_{Alm} and X_{Prp} increase and X_{Grs} decreases in garnet toward biotite (X_{Alm}: 0.6 - 0.73; X_{Prp}: 0.10 - 0.17; X_{Grs}: 0.30 - 0.10).	Eclogite facies	Clockwise	SSDC	-	Domainal equilibration (extent of which is determined by the amount of deformation) and wide variation in composition of peak phases precludes application of thermobarometry
WM83	Metagabbro, metatroctolite	Adirondack Mountains, New York.	Ilm - Pl	*Ilm* | ±Bt | ±Hbl | ±Grt | *Pl*	Corona thickness: *< 100 µm* Garnet vermicule size: *< 50 µm* Vermicule spacing:-- Vermicule Shape: *Columnar Opx and Bt oriented perpendicular layer boundaries*	No systematic zoning observed.	700 - 800ºC and 8 ± 1 kbar from equilibrium assemblages in host rocks	No *P-T* path suggested	SEQ	-	Open system invoked for mass balance. Polymetamorphic history, with a high pressure event following low pressure metamorphism.
B01	Granodiorite	Dora-Maira Massif, Western Alps	*Corona 1:* *Bt - Qtz* *Corona 2:* *Bt - Kfs* *Corona 3:* *Bt - Pl*	*Corona 1:* *Bt* | Grt | *Qtz* *Corona 2:* *Bt* | Grt | Grt+Qtz | Phg+Qtz | *Kfs* *Corona 3:* *Bt* | Grt | Grt+Jd | *Pl*	Corona thickness: *Corona 1: 5 - 40 µm* *Corona 2: Layer 1: 10 - 120 µm; Layer 2: 60 µm; Layer 3: 100 µm* *Corona 3: Layer 1: -; Layer 2: < 100 µm* Garnet vermicule size: *2 - 50 µm* Vermicule spacing:-- Vermicule Shape: *Vermicular garnet to rod-like Phg* Orientation: *Perpendicular layer boundaries*	Disequilibrium. *Corona 1:* Garnet weakly zoned (no more detail provided). *Corona 2:* Garnet weakly zoned (no more detail provided). *Corona 3:* Garnet asymmetrically zoned with Ca increasing and Fe+Mg decreasing toward Pl.	Eclogite facies. Minimum conditions of: 650 °C and 24 kbar, based on comparison between measured and modelled equilibrium compositions of garnet	Clockwise	SSDC	-	Sectoral corona development around biotite depending on immediately adjacent phase. Each corona type represents different *P-T* conditions at which that corona-forming reaction is overstepped.
A98	Metabasic granulite	Yenisey Ridge, Siberia	Pl - Pgt (now Opx+Cpx)	*Pl* | Grt | Grt+Qtz | Cpx+Qtz+Grt | *Pgt* (Opx+Cpx exsolution)	Corona thickness: *Layer 1: 440 µm* *Layer 2: 150 µm* *Layer 3: 300 µm* Vermicule size: *10 - 300 µm* Vermicule spacing:-- Vermicule Shape: *Granoblastic-polygonal/interlobate and locally needle/rod-like pyroxenes.* Orientation: *None*	Disequilibrium. Layer 1 Grt is zoned: Fe increases and Ca decreases (X_{Grs}: 0.24 - 0.21; X_{Alm}: 0.54 - 0.60). In layers 3 and 4, Grt X_{Grs} is constant, while X_{Fe} is higher than in layer 1. No systematic zonation in pyroxene observed.	Layer 4 Grt-Opx and Grt-Opx pairs yield 614 - 635 °C at 6 - 10 kbar (retrograde diffusional resetting). Al content in Opx, yields poorly constrained, slightly higher temperatures. Layer 4 Grt, Opx and Pl reactant yields a pressure estimate of 5.8 - 7.5 kbar (Grt-Opx-Pl-Qtz; Bhattacharya et al., 1991).	Clockwise	SSDC	*Open:* $L_{Fe} \approx L_{Mg} \approx L_{Ca} > L_{Al} \approx L_{Si}$	The geobarometry is compromised by chemical potential gradients between phases in layer 4 and Pl reactant.
WM73	Metagabbro	Adirondacks, New York	Ol - Pl	Southwestern Adirondacks: *Ol* | Opx | Cpx+Spl symp | *Pl*	Corona thickness: *< 0.25 mm* Vermicule size: *0.01 - 0.25 mm* Vermicule spacing:-- Vermicule Shape: *Vermicular symplectite and columnar Opx laths* Orientation: *Strongly oriented perpendicular to layer boundaries*	No variation in X_{Mg} of pyroxenes.	Southwestern Adirondacks: marginally > 8 kbar and 800°C	Clockwise	SSDC?	-	-

Table 3.1 continued: Summary of prograde corona occurrences in the literature

Tag	Bulk comp	Location	Reactants	Corona product assemblage	Corona Thickness, Vermicule size, Vermicule spacing	Equilibration	*P, T* of corona formation	Inferred *P-T* path	Layer growth model	Diffusion model	Comments
A01	Hornblendite xenoliths in marble	Ivrea zone, Northern Italy	Hornblendite - Marble	*Hbl+Grt+Cpx* | Cpx | Grt+Cpx | Scp+Cpx | *Cal*	Corona thickness: *Layer 1: 1 - 4 cm* *Layer 2: 3 - 12 cm* *Layer 3: < 2 cm* Vermicule size: *~ 1 mm* Vermicule spacing:-- Vermicule Shape: *Granoblastic-interlobate except at layer boundaries where vermicular symplectite occurs* Preferred Orientation: *Vermicular symplectite strongly oriented perpendicular to layer boundaries, otherwise none*	Disequilibrium. X_{Mg} (0.8 - 0.55) and Tschermak's content in Cpx decreases toward Cal. No variation in Grt composition.	700 - 900 °C and 7 - 10 kbar (independent estimates of peak conditions from pelites)	-	SSDC	Open. A number of mass balance scenarios proposed based on qualitative evidence to constrain boundary fluxes. $L_{SiSi}/L_{CaCa} > 2.5$ and $L_{AlAl}/L_{CaCa} < 10$ and $L_{MgMg}/L_{CaCa} > 1$	Abart et al. (2001) relaxed the constant volume or closure to certain components constraints to evaluate the overall reaction. Rather, they constrained a range of mass balance scenarios for which major element fluxes across boundaries were solved.
BB88	Metapelite and Norite	Hoggar-Iforas granulite unit, Mali	*Corona 1:* Grt - Sil *Corona 2:* Grt - Qtz	*Corona 1:* *Grt* | Crd | Crd+Spl | *Sil* St and younger euhedral Grt appear to replace Crd in a younger post-corona event. *Corona 2:* *Grt* | Opx+Pl symp | Grt_2+Qtz | *Qtz*	Corona thickness: *Corona 1: < 500µm* *Corona 2: < 700 µm* Vermicule size: *5 - 50 µm* Vermicule spacing:-- Vermicule Shape: *Vermicular symplectite and granoblastic-polygonal/interlobate monomineralic layers* Preferred Orientation: *Vermicular symplectite weakly oriented perpendicular to layer boundaries, otherwise none*	*Corona 1:* No zoning in Crd or Spl. Garnet X_{Fe} decreases rimward. *Corona 2:* No systematic zonation. Opx: X_{Fe} = 0.65 - 0.70, X_{Mg} = 0.29 - 0.32 and X_{Ca}= 0.01 - 0.02.	550 - 650 °C and 4.5 - 5.7 kbar (thermobarometry using the assemblage Grt-Spl-Crd-Bt-Pl)	Clockwise isothermal	SEQ	-	The first stage of corona growth involves breakdown of Grt to form Crd + Spl symplectites in the metapelites and Opx + Pl symplectites in the norites. Replacement of Crd + Spl by younger Grt and Sil, as well as the replacement of Opx and Pl symplectite by Grt + Qtz - suggests renewed burial. Thermobarometry yields *P-T* conditions of the latter event. *P-T* path reflects Eburnean decompression, followed by Pan African burial.
C06	Metapelite	Huangtuling granulite, Northern Dabie Orogen, Eastern China	*Corona 1:* Bt - Pl *Corona 2:* Opx - Pl *Corona 3:* Grt - Qtz+liq *Corona 4:* Bt - Pl+Qtz	*Corona 1:* *Bt* | Grt+Qtz | *Pl* *Corona 2:* *Opx* | Grt+Qtz+Bt_2+Pl_2 | *Pl* *Corona 3:* *Grt* | Crd+Opx±Bt±Pl±Spl symp | Qtz+*Melt* *Corona 4:* *Bt* | Crd+Opx+Qtz | *Pl*	Corona thickness: *100 - 200 µm* Vermicule size: *5 - 50 µm* Vermicule spacing:-- Vermicule Shape: *Vermicular symplectite* Preferred Orientation: *Vermicular symplectite weakly oriented perpendicular to layer boundaries*	*Coronas 1 and 2:* X_{Grs} increases toward Pl (from 2 - 3 mol % to 3 - 4 mol%). Opx: Al^{VI} = 0.05 - 0.07 a.p.f.u. and X_{Mg} = 0.59 - 0.63 Garnet: Ti = 0.24 - 0.28 a.p.f.u. and Al^{VI} = 0.12 - 0.17 a.p.f.u. *Corona 3:* Opx: Al^{VI} = 0.08 - 0.12 a.p.f.u. and X_{Mg} = 0.63 - 0.65 Biotite: X_{Mg} = 0.71 - 0.76 No indication of symmetry in zonation.	*Coronas 1 and 2:* 690 - 790 °C and 7.7 - 9.0 kbar *Coronas 3:* 900 - 920 °C and 4.3 - 4.7 kbar *Corona 4:* 860 - 880 °C and 4.0 - 4.4 kbar (Average *PT*, THERMOCALC)	Clockwise	SSDC	-	Coronas formed at unique *P-T* conditions under steady-state conditions during multi-stage metamorphic history. *Coronas 1 and 2:* decompressive cooling on clockwise path (2000 Ma) *Coronas 3 and 4:* renewed burial of granulites (220 Ma) on a second clockwise prograde path. Corona phase compositions broadly determined by composition of local reactants.
I07	Ultramafic	Sefuri Mountains, NW Kyushu, Japan	Ol - Pl	*Corona 1:* *Ol* | Opx | *Pl* *Corona 2:* *Ol* | Hbl+Opx | Hbl+Spl symp | *Pl*	Corona thickness: *Corona 1: < 70 µm* *Corona 2: < 400µm* Vermicule size: -- Vermicule spacing:-- Vermicule Shape: *Corona 1: Columnar Opx* *Corona 2: Granoblastic-polygonal layer 1. Layer 2 comprises vermicular symplectite weakly oriented perpendicular to layer boundaries*	Al cation total decreases (1.21 - 0.48; 23 O's) and X_{Mg} increases (0.88 - 0.91) in Hbl toward Ol in layer 1. X_{Al} in Opx increases toward Pl (0.06 - 0.11) in layer 1.	600 - 700 °C, 5 kbar (Hbl-Opx thermometry on mineral pairs from layer 2 - employing Gibbs method for Fe-Mg exchange between Hbl and Opx)	Not described	SSDC	-	Open system removal of MgO from the local corona volume, stabilises Opx in the corona

Table 3.1 continued: Summary of prograde corona occurrences in the literature

Tag	Bulk comp	Location	Reactants	Corona product assemblage	Corona Thickness, Vermicule size, Vermicule spacing	Equilibration	*P, T* of corona formation	Inferred *P-T* path	Layer growth model	Diffusion model	Comments
MCC03	Metapelite	Makhavinekh Lake Pluton	Grt - Qtz+Fsp	*Grt* | Crd+Opx | Pl | Opx | *Qtz+Fsp*	Corona thickness: *< 50 µm (6 km from pluton) to > 1000 µm (adjacent to pluton)* Vermicule size: *< 10 µm (6 km from pluton) to 250 µm (adjacent to pluton)* Vermicule spacing:-- Vermicule Shape: *Elongate and vermicular furthest from contact becoming more equant toward pluton* Orientation: *Rods strongly aligned perpendicular to garnet substrate*	Al_2O_3 wt % and X_{Mg} of Opx increases toward reactant garnet. Magnitude of difference dependent on distance to pluton. Max ΔAl wt% = 0.8 wt%; Max ΔX_{Mg} = 0.05. Overall Opx more Fe-rich and Al-rich toward pluton. Intracrystalline zonation toward lower Al wt% and X_{Mg} values at margins of vermicules.	Grt-Opx Al-solubility thermometry: Contact: 785 - 875 °C at 5 kbar At 6km: 650 - 750 °C	Contact aureole	SSDC	-	Progressive replacement of garnet toward pluton contact
IO02	Pelitic and mafic granulites	Taylor Brook Gabbro Complex	*Corona 1:* Sil - Grt - Qtz *Corona 2:* Grt - Qtz	*Corona 1:* *Grt* | Spl + Crd | *Qtz+Sil +Grt* *Corona 2:* *Grt* | Pl | Opx | *Qtz*	Corona thickness: *Corona 1: < 500 µm* *Corona 2: < 100µm* Vermicule size: *Corona 1:* < 300 µm *Corona 2:* < 50 µm Vermicule spacing:-- Vermicule Shape: *Corona 1: Tortuous, contorted lamellar symplectite* *Corona 2: Granoblastic-polygonal* Orientation: *Lamellae weakly aligned perpendicular to garnet substrate*	No zonation described.	Grt-Opx-Pl-Qtz thermobarometry on corona phases in metabasite yields a *P-T* estimate of 4.4 kbar at 615ºC. Coronas in tonalitic gneiss yield a slightly higher *P* and *T* of 4.7 kbar at 645ºC.	Contact aureole	SSDC	-	-
BBOO	Metapelite	Mafic Complex Contact Aureole	Crd - Kfs	*Crd* | Bt+Sil+Qtz | *Kfs*	Corona thickness: *< 200µm* Vermicule size: < 30 µm Vermicule spacing: > 5 µm Vermicule Shape: *Vermicular symplectite*	No zonation described.	-	Contact aureole	-	-	-
WMP04	Metapelite	Ross of Mull Contact Metamorphic Aureole, Scotland	*Corona 1:* Ky - Bt - Qtz *Corona 2:* Grt - Qtz - Ms	*Corona 1:* *Ky* | Crd + Ms | *Qtz+Bt* *Corona 2:* *Grt* | Crd + Bt | *Qtz+Ms*	Corona thickness: *Corona 1: < 350 µm* *Corona 2: < 1000µm* Vermicule size: *Corona 1:* - *Corona 2:* < 20 µm Vermicule spacing:-- Vermicule Shape: *Corona 1: Fibrous intergrowth* *Corona 2: Elongate, anhedral biotite laths in cordierite* Orientation: *Vermicules weakly aligned perpendicular to reactant substrate*	Zonation not described. Apparently in equilibrium.	*P-T* estimates based on relative stability of phases on *P,T* grids	Contact aureole	-	-	=
L04	Metatroctolite	Buck Creek Ultramafic body, North Carolina Blue Ridge	Ol - Pl	*Ol* | Opx | Cpx+Spl symp | *Pl* *Ol* | Opx | Cpx+Hbl symp | *Pl* *Ol* | Opx | Cpx+Spr symp | *Pl*	Corona thickness: *0.5 - 0.75 mm* Vermicule size: -- Vermicule spacing:-- Vermicule Shape: *Vermicular symplectite and elongate or columnar Opx laths* Orientation: *Strongly oriented perpendicular to layer boundaries*	Equilibrium. No variation in composition.	700 - 900 °C and > 9 kbar	-	SSDC	Closed. No diffusion modelling performed. SVD analysis concludes Hbl of primary metamorphic origin - not retrograde after Cpx.	Overall corona reaction modelled by SVD (Singular Value Decomposition) matrix technique. Possible mass balance reactions are generated by SVD technique. A successful model is one that reproduces a sensible overall reaction with residuals that match expected analytical errors (Lang et al., 2004). *Closed system approximation possibly invalid.*

Table 3.1 continued: Summary of prograde corona occurrences in the literature

Tag	Bulk comp	Location	Reactants	Corona product assemblage	Corona Thickness, Vermicule size, Vermicule spacing	Equilibration	*P, T* of corona formation	Inferred *P-T* path	Layer growth model	Diffusion model	Comments
DO2	Mafic granofels	Arthur River Complex at Mt Daniel, Fiordland, New Zealand	Hbl - Czo	*Hbl* | Cpx + Ky + Qtz + Pl | *Czo*	Corona thickness: *< 500 µm* Vermicule size: *< 60 µm* Vermicule spacing:-- Vermicule Shape: *Irregular, elongate, euhedral laths of Ky embedded in Cpx and Qtz* Orientation: *No preferred orientation*	No zonation - equilibrium.	The assemblage garnet, kyanite, plagioclase and quartz yielded pressure estimates of 13.2 kbar and temperature estimates of 700 °C using conventional thermobarometer of Newton and Perkins, 1982.	Contact aureole	-	-	-
D97	Metapelite	Chimakurthy mafic-ultramafic complex aureole, Eastern Ghats Belt, India	Spl - Crd	*Corona 1:* *Spl* | Grt + Sil + Crd | *Crd* *Corona 2:* *Grt* | Opx + Sil + Spl	Corona thickness: *Corona 1: < 75 µm; Corona 2: < 230µm* Vermicule size: *Corona 1: < 15 µm; Corona 2: < 10 µm* Vermicule spacing: -- Vermicule Shape: *Corona 1: Irregular, lenticular sillimanite needles in cordierite intergrown with 'spongy' garnet. Corona 2:Rod-like intergrowth of Opx, Sil and Spl* Orientation: *Orthopyroxene vermicules aligned perpendicular to layer boundaries*	No zonation described.	*P-T* grid constraints on pressure: 5 - 6 kbar with cooling from 1000 °C.	Contact aureole	-	-	-

JC90: Johnson and Carlson, (1990); N83: Nishiyama, (1983); J04: Johnson et al., (2004); WC97: White and Clarke, (1997); I93: Indares, (1993); JF88: Joesten and Fisher, (1988); ABE92: Ashworth et al., (1992); K87: Koons et al., (1987); WM83: Whitney and McLelland, (1983); A98: Ashworth et al., (1998); B01: Bruno et al., (2001); WM73: Whitney and Mclelland, (1973); A01: Abart et al., (2001); BB88: Boullier and Barbey, (1988); C06: Chen et al., (2006); I07: Ikeda et al., (2007); MCC03: Mcfarlane et al., (2003); IO02: Ings and Owen, (2002); BB00: Barboza and Bergantz, (2000);WMP04: Wheeler et al., (2004); L04: Lang et al., 2004; D02: Daczko et al., (2002); D97: Dasgupta et al., (1997).

Table 3.2: Summary of retrograde corona occurrences in the literature

Tag	Bulk comp	Location	Reactants	Corona product assemblage	Corona Thickness, Vermicule size, Vermicule spacing	Equilibration	*P, T* of corona formation	Inferred *P-T* path	Layer growth model	Diffusion model	Comments
CJ91	Metagabbro	Llano Uplift, Central Texas	*Corona 1:* Grt - Qtz *Corona 2:* Grt - Omp	*Corona 1:* *Grt* | Pl+Mgt | Opx+Aug | *Qtz* *Corona 2:* *Grt* | Pl+Prg symp | Mg-Hbl | Pl+Mg-Hbl+Opx symp | *Omp*	*Corona 1:* Corona thickness: *Pl = 60 µm; Opx+Hbl = 20 µm* Vermicule size: *< 5 - 10 µm* Vermicule spacing:-- Vermicule Shape: Pl+Mgt - *granoblastic-polygonal; Opx+Aug - columnar* Orientation: *Columnar Opx+Aug perpendicular layer boundaries* *Corona 2:* Corona thickness: *200 µm* Vermicule size: *< 2 µm - 40 µm* Vermicule Shape: *Granoblastic-polygonal Pl; vermicular/rod-like Hbl and Opx* Orientation: *Weakly perpendicular to layer boundaries*	Disequilibrium. Pl less calcic and amphibole Fe/Mg and Al/Si ratios decrease toward quartz/omphacite (An_{35}-An_{18}).	-	ITD	SSDC	Open Grt-Qtz: $L_{Fe} > L_{Mg} \geq L_{Ca} \geq L_{Al} \geq L_{Si}$ Grt-Omp: $L_{Na} \approx L_{Fe} > L_{Mg} \geq L_{Si} \geq L_{Ca} \geq L_{Al}$	
CPG89	Metapelite	MacRobertson Land, Antarctica	*Corona 1:* Crd - Spl *Corona 2:* Spl - Matrix (Grt+Sil+Qtz+Kfs) *Corona 3:* Ilm - Grt	*Corona 1:* *Spl* | Mgt | Sil | *Crd* *Corona 2:* *Spl* | Grt+Sil+Crd | *Grt+Sil+Qtz+Kfs* *Corona 3:* *Ilm* | Sil | *Grt*	Corona thickness: *Corona 1: 200 µm* *Corona 2: < 120 µm* *Corona 3: 30 - 120 µm* Grain size: *< layer thickness* Grain shape: *Granoblastic-polygonal* Orientation: *None*	-	-	IBC following ITD	SSDC	-	-
K03	Metapelite	Mather Paragneiss, Rauer Group, Antarctica	*Corona 1:* Grt - Qtz *Corona 2:* Grt - Bt *Corona 3:* Sil - Opx	*Corona 1:* *Grt* | Crd+Opx symp | Opx | *Qtz* *Corona 2:* *Grt* | Crd+Opx symp | Pl | *Bt* *Corona 3:* *Sil* | Crd | *Opx*	Corona thickness: *< 0.5mm* Grain size: -- Grain shape: -- Orientation: *Symplectite phases perpendicular to layer boundaries*	Disequilibrium. Crd X_{Mg} varies across symplectite - generally not systematically, but X_{Mg} may increase toward Opx. No variation in Opx composition.	750 - 800 ºC and 7 - 8 kbar, (modal *P-T-X* relationships from pseudosections)	Decompressive cooling on clockwise path	SSDC	-	-
WPC02	Fe-rich metapelites	Musgrave Block, Central Australia	Grt - Matrix (Sil, Qtz, Kfs, Bt)	*Grt* | Spl+Qtz+Grt | *Matrix* Grt encloses Spl in corona	Corona thickness: *< 0.5mm* Grain size: *0.05 - 0.2 mm* Grain shape: *Granoblastic-polygonal/interlobate* Orientation: *None*	Equilibrium.	800 - 850 ºC and 5.5 - 6.0 kbar (*P-T-X* relationships from pseudosections)	Clockwise path with minor decompression dominated by cooling	SEQ	-	Coronas develop in response to changing modes in a high variance equilibrium assemblage. No univariant reaction is crossed. Garnet is still stable. Implies that decompression implied by this texture may have been over-estimated in other terranes (Harley, 1989).
KS99	Mg-rich metapelites	Highland Complex, Hakurutale, Sri Lanka	*Corona 1:* Grt - Qtz *Corona 2:* Grt - Qtz *Corona 3:* Grt - Bt *Corona 4:* Sil - Opx/Grt (SiO_2 Deficient EBC)	*Corona 1:* *Grt* | Opx+Sil symp | Opx | *Qtz* *Corona 2:* *Grt* | Opx+Crd±Spr symp | Opx | *Qtz* *Corona 3:* *Grt* | Opx+Pl±Crd symp | *Bt* *Corona 4:* *Sil* | Crd±Spr symp | Crd | *Opx/Grt*	Corona Thickness: *Corona 1: < 0.5mm* Grain Size: *Corona 1:* *Coarse granoblastic-polygonal grains < 0.2mm; symplectite vermicules: 10 - 50 µm* Grain shape: *Symplectite: vermicular* *Monomineralic layers: granoblastic-polygonal* Orientation: *Symplectite vermicules weakly aligned perpendicular to layer boundaries*	Disequilibrium. *Corona 1:* Opx: X_{Mg} = 0.76 - 0.84; X_{Al} = 0.09 - 0.15 *Corona 2:* Opx: X_{Mg} = 0.76 - 0.83; X_{Al} = 0.12 - 0.17 No systematic variation noted.	810 ºC and 7.5 kbar. TWQ *P-T* estimate on Grt, Qtz, Opx, Crd assemblage. Assumed Grt + Qtz in equilibrium with products.	Clockwise path with ITD	SSDC	-	

Table 3.2 continued.: Summary of retrograde corona occurrences in the literature

Tag	Bulk comp	Location	Reactants	Corona product assemblage	Corona Thickness, Vermicule size, Vermicule spacing	Equilibration	*P, T* of corona formation	Inferred *P-T* path	Layer growth model	Diffusion model	Comments
N02	Mafic, aluminous pelites	Thor-Odin Dome, Shuswap metamorphic core complex, British Columbia	Ged - Ky	*Ged* | Crd | Crd+Spl sympl | Crd+Crn sympl | *Ky*	Corona thickness: *Layer 1: < 350 µm* *Layer 2: < 900 µm* *Layer 3: pseudomorphs kyanite* Vermicule size: *25 - 350 µm* Vermicule spacing: *20 µm* Vermicule Shape: *Vermicular symplectite; granoblastic-polygonal/interlobate in Crd moat* Orientation: *Vermicular symplectite weakly oriented perpendicular to layer boundaries, otherwise none*	Equilibrium. No variation in any phases noted.	*P* < 5 kbar and *T* ~ 750 °C. Equilibria constrained with TWQ and conventional thermobarometers.	Rapid isothermal decompression on a clockwise path	SSDC	-	
H06	Metapelite	Leverburgh Belt, South Harris, Scotland	Grt - Qtz	*Grt* | Crd+Opx symp | Opx | *Qtz*	Corona thickness: *Layer 1: < 200 µm* *Layer 3:< 50 µm* Vermicule size: 10 - *50 µm* Vermicule spacing: *25 µm* Vermicule Shape: *Rod-like symplectite; columnar Opx in layer 2.* Orientation: *Vermicular symplectite weakly oriented perpendicular to layer boundaries*	Disequilibrium. No systematic variation described. Opx: *y*(Opx) = 0.02 - 0.08 X_{Mg} = 0.71 - 0.78 Cordierite: X_{Mg} = 0.89 - 0.92	*P* ~ 9 kbar and *T* ~ 870 °C.	Isothermal decompression on anti-clockwise path	SSDC	-	
G80	Metapelite	Enderbyland, Antarctica	Spr - Qtz	*Spr* | Sil | Opx | *Qtz*	Corona Thickness: *< 0.5mm*	-	7 ± 1 kbar; 900 ± 30 °C	Isobaric cooling on anticlockwise path	SSDC	-	-
B04	Troctolitic gabbro	Snowbird Tectonic Zone, Western Canadian Shield	Grt - Cpx	*Grt* | Opx+Pl symp | Spl+Cpx+Opx symp | *Omp* *Grt* | Prg+Pl | Pl | Opx+Pl | *Omp*	Corona thickness: *Layer 1: < 70 µm* *Layer 2: 20 µm* *Layer 3: 50 µm* Vermicule size: *< 50 µm* Vermicule spacing:-- Vermicule Shape: *Elongate Prg laths; euhedral Opx rhombs* Orientation: O*riented perpendicular to layer boundaries*	Disequilibrium. Marked zonation in Pl (An_{91} adjacent Grt to An_{44} at corona margin). No variation in amphibole, orthopyroxene or clinopyroxene compositions documented.	850 - 855 °C at 10 - 12 kbar (two pyroxene thermometry) 810 °C and 12 kbar (Grt-Opx-Pl-Qtz equilibria - TWQ; Grt rim and symplectite compositions)	Isothermal decompression on clockwise path	SSDC?	-	Corona mineralogy depends on availability of H_2O to form amphibole. The use of corona plagioclase composition in TWQ thermobarometry may not be valid.
ACK07	Metapelite	NVP (Neocene Volcanic Province), El Hoyazo, Spain	Grt - Matrix (Bt+Sil+Pl)	*Grt* | Spl+Crd+Kfs+Melt (glass) | *Matrix* Pl rinds separate Spl from Crd.	Corona thickness: *< 150 µm* Vermicule size: *< 50 µm* Vermicule spacing:-- Vermicule Shape: *Euhedral Spl and granoblastic-interlobate Crd* Orientation: *No preferred orientation*	Equilibrium. No systematic variation in spinel or cordierite composition.	820 ± 50 °C, 4.5 ± 0.6 kbar (ternary feldspar thermometry, Grt-Crd thermobarometry, GASP barometry)	Rapid decompression during eruption followed by isobaric cooling	SSDC/SEQ	-	Plagioclase rind between cordierite and spinel is attributed to isobaric cooling post-eruption.
T06	Metapelite	Mather Paragneiss, Rauer Group.	1) Grt 2) Grt - Melt 3) Sil - Opx 4) Grt - Qtz 5) Grt - Cpx+Hbl	1) *Grt* | Spr+Opx+Crd symp 2) *Grt* | Bt+Crd symp | *Melt* 3) *Sil* | Spr+Crd symp | *Opx* 4) *Grt* | Crd+Opx symp | Opx | *Qtz* 5) *Grt* | Opx_1+Pl | Opx_2+Pl+Mgt | *Cp x+Hbl*	*Corona 5:* Corona thickness: *Layer 1: < 2 mm* *Layer2: 1 mm* Grain size: *< 0.5 mm* Grain shape: *Opx_1 is vermicular, Opx_2 is euhedral and columnar* Orientation: *Symplectite vermicules strongly aligned perpendicular to layer boundaries*	No variation in corona cordierite observed. Symplectitic Orthopyroxene: X_{Mg}= 0.71 - 0.72; 4.1 - 4.2 Al_2O_3 wt.%. Symplectitic Spr: Si = 1.36 - 1.39 a.p.f.u.	Two groups of post-peak *P-T* estimates: 980 - 1010 °C (Grt-Opx thermobarometry) and ~10 kbar; ~ 800 °C and ~ 7 kbar (Grt-Bt thermometry).	Clockwise path with near isothermal decompression under ultrahigh *T* followed by decompression cooling	1-4) SSDC 5) SEQ	-	

Table 3.2 continued: Summary of retrograde corona occurrences in the literature

Tag	Bulk comp	Location	Reactants	Corona product assemblage	Corona Thickness, Vermicule size, Vermicule spacing	Equilibration	*P, T* of corona formation	Inferred *P-T* path	Layer growth model	Diffusion model	Comments
G72	Olivine pod in anorthosite	Sognefjord and Bergen, Norway	Ol - Pl	*Type 1:* *Ol* | Opx | Cpx | Grt | Cpx+Spl | *Pl* *Type 2:* *Ol* | Opx | Cpx | Grt+Cpx+Spl | *Pl* *Type 3:* *Ol* | Cpx | Grt+Cpx+Spl | *Pl* *Type 4:* *Ol* | Cpx | Pl | Grt | *Pl*	Corona Thickness: *Type 2:* *Opx: 6 - 15 mm; Cpx: 4 - 6 mm; Grt: 7 - 15 mm;* *Type 3:* *Opx: 1 cm; Cpx: 5 mm; Grt: 5 - 8 mm;* *Type 4:* *Opx: 3 mm; Cpx: 1 mm; Grt: 2 mm;* Grain size: -- Grain shape: -- Orientation: --	Disequilibrium. *Type 2 corona:* Bergen: Opx strongly zoned - Al content and X_{Fe} increase from olivine toward Pl. Garnet strongly zoned - Ca decreases and Mg+Fe increases towards Cpx. Sognefjord: All phases homogeneous. *Type 3 corona:* All phases homogeneous, except garnet where Ca decreases toward Cpx. *Type 4 corona:* Mg and Ca increase in Cpx toward plagioclase layer. Ca decreases in the garnet layer toward plagioclase layer.	1000 ºC and 12 kbar (Grt-Cpx thermometry) Cooling to 500 ºC	Cooling from peak igneous *T* at high pressure	SEQ	-	Coronas 1 - 4 are considered to represent transient, increasingly more evolved stages of corona development on the *P-T* path.
MA83	Olivine metagabbro	NE, Scotland	Ol - Pl	*Ol* | Opx | Hbl | Hbl+Spl/An symp | *Pl*	Corona thickness: *Opx: 70 µm; Hbl: 30 µm; Hbl+Spl: 100 µm* Spinel vermicule size: *0.5 - 5 µm (max 30 µm)* Vermicule spacing:-- Vermicule Shape: *Subhedral, columnar Hbl+Opx; vermicular spinel* Preferred Orientation: *Perpendicular layer boundaries*	Disequilibrium. Al content and X_{Fe} of Opx and Hbl increase toward Pl reactant. Opx: Al_{cat} = 0.03 - 0.07; X_{Fe} = 0.26 - 0.28 Hbl: Al_{cat} = 2.72 - 2.77; X_{Fe} = 0.28 - 0.26	Amphibolite facies. No quantitative thermobarometry	Cooling from peak igneous *T*	SSDC	Open: $L_{Fe} \geq L_{Mg} \geq L_{Ca} > L_{Al} > L_{Si}$	
G88	Metagabbro	Central Gneiss Belt, Western Grenville Province, Ontario.	Ol - Pl	*Ol* | Opx | Cpx | ±Amph | Grt | *Pl*	Corona thickness: *Overall 250 - 500 µm* Vermicule/Grain size: *Not resolvable* Vermicule spacing: *Not resolvable* Vermicule Shape: *Granoblastic-polygonal Grt, columnar Cpx and Opx* Preferred Orientation: *Opx and Cpx oriented perpendicular to layer boundaries*	Disequilibrium. Opx and Cpx zoned w.r.t. Al - increases from 1.4 - 1.8 wt% toward Pl. Variable Si and Al in amphibole (± 2 wt%). Al/Si ratio decreases in the symplectite toward olivine. Garnet compositions are homogeneous.	8 - 10 kbar and 700 - 750 ºC from equilibrium assemblages is in host gneisses	Cooling from peak igneous *T* at high pressure	SSDC - with back reaction and re-equilibration.	Closed: Cross coefficient terms L_{CaMg} and L_{CaFe} introduced to stabilise garnet in symplectite. Semi-quantitative results only with $L_{Fe2+} \approx L_{Mg} > L_{Al} > L_{Si}$ and $L_{Mg}/L_{Na} < 6 - 8$. $L_{Ca}/L_{Al} < 1.5 - 2.0$. $L_{Mg}/L_{Ca} < 4 - 6$	The closed system assumption forced Grant to assume a 'fictive' non-stoichiometric plagioclase composition to accommodate excess Ca required to stabilise Cpx-bearing coronas. The garnet layer was not included in the SSDC model since it was believed to post-date the main corona.
J86	Troctolitic gabbro	Risor, Norway	Ol - Pl	*Ol* | Opx | Opx+Spl symp | Hbl+Spl symp | *Pl* *Ol* | Opx | Hbl | Hbl+Spl symp | *Pl*	Corona thickness: *Opx layer: 72 - 105 µm; Opx+Spl: 10 - 20 µm;* *Hbl+Spl: 110 - 205 µm* Vermicule size: *Spl:1 - 2 µm* Vermicule spacing:-- Vermicule Shape: *Opx and Hbl: columnar; Spl: needles/rods* Orientation: *Spl rods perpendicular layer boundaries*	Equilibrium - no variation described.	-	Primary coronas magmatic in origin, followed by secondary solid-state annealing	SEQ	Closed: none stable	Diffusional instability of primary coronas drives secondary annealing to produce stable secondary solid-state coronas. Remodelled successfully by Ashworth (1986), consistent with emplacement into regional metamorphic terranes and cooling from igneous temperatures.
WM73	Metagabbro	Adirondacks, New York	Ol - Pl	Adirondack Highlands: *Ol* | Opx | Cpx | Pl | Grt(±Cpx±Hbl) | *Pl*	Corona thickness: *Overall 500 - 700 µm* Vermicule/Grain size: *not resolvable* Vermicule spacing: *not resolvable* Vermicule Shape: *Granoblastic-polygonal Grt; columnar Cpx and Opx* Preferred Orientation: *Opx and Cpx oriented perpendicular to layer boundaries*	Jd/Ts in Cpx decreases from Ol toward Pl (ascribed to formation under different *P-T* conditions in sequential model). No variation in X_{Mg} of pyroxenes.	Adirondack Highlands: ~8 kbar and 800°C	Cooling from peak igneous temperatures	SEQ	-	Close association of metagabbros with anorthosite argues against depression of relatively buoyant crust to depths sufficient to explain prograde formation of coronas. Garnet-bearing coronas in the Northern Adirondacks reflect higher pressures during corona formation. Absence of garnet locally in coronas is attributed to kinetic nucleation constraints.

Table 3.2 continued: Summary of retrograde corona occurrences in the literature

Tag	Bulk comp	Location	Reactants	Corona product assemblage	Corona Thickness, Vermicule size, Vermicule spacing	Equilibration	*P, T* of corona formation	Inferred *P-T* path	Layer growth model	Diffusion model	Comments
D89	Metapelite	Central Zone, Limpopo Belt, Zimbabwe	*Corona 1:* Grt - Krn *Corona 2:* Crn - Krn *Corona 3:* Crn - Ged	*Corona 1:* *Grt* | Ged+Spl | Ged+Spr | Spr+Crd | *Krn* *Corona 2:* *Crn* | Spl | Spr+Crd | *Krn* *Corona 3:* *Crn* | Spl | Spr+Crd | Crd | *Ged*	Corona thickness: Corona 1: *Layer 1: < 200µm; Layer 2: ~ 250 µm; Layer 3: < 200µm* *Corona 2: < 750 µm* *Corona 3: Layer 1: < 1000 µm; Layer 2: 500 µm; Layer 3: < 700 µm* Grain size: *< maximum layer thickness* Grain shape: *Symplectite: vermicular* *Monomineralic layers : granoblastic-polygonal* Orientation: *Symplectite vermicules radially aligned in sectors (not always perpendicular to layer boundaries)*	Equilibrium: No variation described in any phases.	700 - 800 °C; 3.5 - 5 kbar (MASH equilibria: Grt-Spr-Spl-Crd thermobarometry)	Isothermal decompression	SEQ	-	-
LAL87	Metapelite	Paderu, Southern India	*Corona 1:* Spr - Qtz *Corona 2:* Spl - Qtz *Corona 3:* Spr - Sil *Corona 4:* Opx - Melt	*Corona 1:* *Spr* | Sil | Opx/Crd | *Qtz* *Corona 2:* *Spl* | Spr | Sil | *Qtz* *Spl* | Spr | Opx | *Qtz* *Spl* | Sil | Opx | *Qtz* *Spl* | Spr | Sil | Grt/Opx | *Qtz* *Corona 3:* *Spr* | Opx | *Sil* *Corona 4:* *Opx* | Bt+Qtz symp | *Melt*	-	No systematic variation recorded for any corona phases.	900 ± 60 °C and 6.5 ± 0.7 kbar to 760 ± 50°C and 5.0 ± 0.6 kbar (Grt-Opx thermobarometry) and relationships on the FMASH petrogenetic grid	Decompressive cooling on clockwise path.	SSDC	-	Variation in corona mineralogy dependent on topology of petrogenetic grid and local variation in bulk composition (μ_{FeO}, μ_{Fe2O3} and μ_{H2O}).
O04	Metapelite	Kontum Massif, Central Vietnam	Grt - Qtz	*Grt* | ±Prp±Spl symp | Crd+Opx symp | Opx | ±Pl±Kfs | *Qtz*	Corona thickness: *Symp layer: < 400 µm; Mono Opx: < 100 µm;* Vermicule size: *20 - 100 µm* Vermicule spacing: *10 - 30 µm* Vermicule Shape: *Symplectite: vermicular* *Monomineralic Opx: Columnar/blocky; Spl: needles/rods* Orientation: *Weakly oriented perpendicular to layer boundaries*	Disequilibrium. Zonation noted but not described. Symplectite Opx: X_{Mg} = 0.62 - 0.70; 5.8 - 7.6 Al_2O_3 wt% Crd: X_{Mg} = 0.82 - 0.84 Spl: X_{Mg} = 0.67 - 0.71 Mono Opx: X_{Mg} = 0.67 - 0.71; 4.7 - 5.3 Al_2O_3 wt%	Cooling from 9 kbar, 1000 °C to 6.5 kbar, 800 °C from FMASH petrogenetic grid, X_{Al} and X_{Mg} contours.	ITD on clockwise path	SEQ	-	Assumed preserved metastable equilibria in corona represent discrete *P-T* conditions.
T04	Metapelite	Ganguvarpatti, Southern India	*Corona 1:* Grt - Matrix *Corona 2:* Grt - Qtz	*Corona 1:* *Grt* | Opx±Spr±Spl | *Matrix* (composite symplectite) *Corona 2:* *Grt* | Opx+Crd | *Qtz*	Corona Thickness: *Corona 1: < 300 µm* *Corona 2: Layer 1: < 1000 µm* Grain size: 50 - 100 *µm* Grain shape: *Symplectite: needle-like Spr rods* *Monomineralic layers: granoblastic-polygonal* Orientation: *Symplectite Spr vermicules strongly aligned radially w.r.t layer boundaries Opx vermicules perpendicular to layer boundaries*	Near equilibrium. Minor asymmetrical zonation in cordierite described with highest X_{Mg} values adjacent to garnet (X_{Mg}: 0.85 - 0.89). Spr X_{Mg}: 0.73 - 0.75 Spl X_{Mg}: 0.41 - 0.44 Opx in corona 1: Al_2O_3 contents 7.6 - 8.2 wt %. Opx in corona 2: Al_2O_3 contents 6.9 - 7.5 wt %.	Crd+Opx symp: 950 - 990 °C, > 8kbar Crd±Spr±Spl symp: 850 - 900 °C, 8 kbar (X_{Mg} and X_{Al} Opx thermobarometry, Hensen and Harley, 1990)	Steep decompressive cooling on clockwise path	SSDC	-	-

Table 3.2 continued: Summary of retrograde corona occurrences in the literature

Tag	Bulk comp	Location	Reactants	Corona product assemblage	Corona Thickness, Vermicule size, Vermicule spacing	Equilibration	*P, T* of corona formation	Inferred *P-T* path	Layer growth model	Diffusion model	Comments
ZH07	Metapelite	Vestfold Hills, East Antarctica	*Corona 1:* Pl - Opx *Corona 2:* Grt - Pl	*Corona 1:* Pl_1 | Pl_2 | ±Kfs | Grt_{2b}+Qtz | *Opx* *Corona 2:* *Grt* | Grt_{2a}+Qtz | Pl_2	Corona Thickness: *Corona 1:* *Layer 1: ?* *Layer 2: < 30 µm* *Layer 3: < 170 µm* *Corona 2:* *Layer 1: < 100 µm* Grain size: 5 - 100 *µm* Grain shape: *Symplectite: granoblastic* *Monomineralic layers: granoblastic-polygonal* Orientation: *Symplectite vermicules weakly aligned perpendicular to layer boundaries*	Grt_{2a} zoned radially w.r.t. Ca, Fe and Mg. $Alm_{65-68}Grs_{10-15}Prp_{19-21}Sps_{1-2}$, with X_{Mg} of 0.21 - 0.24.	600 - 680 °C, 6 - 8 kbar (Garnet-Opx thermometry, GAFS barometry)	Isobaric cooling	SSDC	-	-
M98	Fayalite granites	Lofoten Islands, Norway	*Corona 1:* Fa/Mgt - Pl *Corona 2:* Fa/Mgt - Kfs	*Corona 1:* *Fa* | Opx | Grt+Opx | *Pl/Kfs* *Corona 2:* *Fa* | Opx | Amph | *Pl/Kfs* (Opx+Grt layers thinner and Opx:Grt in Opx+Grt layer is higher adjacent to Kfs than Pl) *Mgt* | Grt+Opx | *Fsp* *Mgt* | Amph | *Fsp*	Corona Thickness: *Corona 1:* *Layer 1: < 50 µm* *Layer 2: < 20 µm* Grain size: 2 - *20 µm* Grain shape: *Symplectite: granoblastic* *Monomineralic layers : polygonal granoblastic* Orientation: *Symplectite vermicules aligned perpendicular to layer boundaries*	Disequilibrium. Garnet only exhibits zonation, becoming more calcic (X_{Ca}: 0.09 - 0.15) and magnesian (X_{Mg}: 0.95 - 0.97) toward feldspar.	780 - 840 °C and 4 - 10 kbar (Grt-Cpx-Opx-Pl thermobarometry). Large variation in pressure is due to variation in garnet composition across the corona.	Cooling from peak igneous temperatures	SSDC	Open system model with constant volume constraint: $L_{Fe}>L_{Si}>L_{Mg}>L_{K}>L_{Na} >> L_{Ca}>L_{Mn}>L_{Al}$	Markl et al. (1998) is first study to constrain relative diffusion coefficients of major components in granulite facies granitic rocks.
BPS87	Metapelite	Errabiddy, Western Australia	*Corona 1:* Grt - Ged *Corona 2:* Ky - Ged	*Corona 1:* *Grt* | Crd+Ged_2 | *Ged* *Corona 2:* *Ky* | St | Crd | *Ged*	Corona thickness: *< 100 µm* Grain size: *20 µm* Grain shape: *Symplectite: granoblastic* *Monomineralic layers : granoblastic-polygonal* Orientation: *Symplectite vermicules aligned perpendicular to layer boundaries*	*Corona 1:* X_{Fe} in Crd decreases from 0.17 near Grt to 0.1 - 0.13 adjacent to Ged. Ged X_{Fe} 0.37 - 0.47; Al^{IV} 1.3 - 2.2. *Corona 2:* X_{Fe} in Crd increases toward Ged from 0.10 to 0.16. Ged X_{Fe}: 0.26 - 0.36	600 - 650°C, 4 - 6 kbar (*P-T-X* phase equilibria)	Clockwise reheating of originally high-grade rocks, followed by isothermal uplift	SSDC	-	Variations in the proportions of cordierite and staurolite are directly related to the X_{Fe} and Ca composition of gedrite reactant.
BKO03	Metapelite	Epupa Complex, NW Namibia	Grt - Qtz	*Grt* | Crd+Opx | Pl | Opx | *Qtz*	Corona thickness: *Layer 1: < 250µm* *Layer 2: < 70 µm* Grain size: *20 - 250 µm* Grain shape: S*ymplectite - lamellar* Orientation: *Symplectite vermicules aligned perpendicular to layer boundaries*	Opx X_{Al} increases toward Grt (Al_{tot}: 0.12 - 0.25). X_{Mg} of Opx and Crd decrease toward Qtz (0.66 - 0.52 in Opx; X_{Fe} 0.87 - 0.81 in Crd) No zonation in Pl.	Stage 1 corona formation: 940 ± 30 °C and 8 ± 2 kbar (Grt-Opx thermometry and Grt-Opx-Pl-Qtz barometry on Grt rim, layer 2 Pl and layer 3 Opx) Stage 2 corona growth: 800 ± 60 °C and 6 ± 2 kbar (Grt-Opx thermometry and Grt-Opx-Pl-Qtz barometry)	Post peak decompression, followed by near isobaric cooling -clockwise retrograde path	SEQ	-	Increase in Al content in Opx toward Qtz inconsistent with diffusion controlled growth, i.e., Al diffusion is rate-limiting. Either Al diffused anomalously quickly in this instance or the Crd+Opx symplectites formed at lower temperature. Thermobarometry potentially applied to disequilibrium compositions.
TM85	Emeries	Cortland Complex, New York	Spr - Qtz	*Spr* | Opx | Sil | *Qtz*	Corona thickness: *< 60 µm* Grain size: *< 60 µm* Grain shape: *Granoblastic-polygonal* No preferred orientation	Disequilibrium. Homogeneous Fe+Mg in Opx. Al content in Opx increases toward Spr.	-	-	SEQ	-	Partial equilibrium attained by Fe+Mg, i.e., inferred to be the most rapidly diffusing components such that chemical potential gradients were eliminated

Table 3.2 continued: Summary of retrograde corona occurrences in the literature

Tag	Bulk comp	Location	Reactants	Corona product assemblage	Corona Thickness, Vermicule size, Vermicule spacing	Equilibration	*P, T* of corona formation	Inferred *P-T* path	Layer growth model	Diffusion model	Comments
TVR06	Metapelite	Central Zone, Limpopo Belt, Zimbabwe	Sil - Ged	*Sil* | Spr±Spl+Crd | Crd | *Ged*	Corona Thickness: *Corona 1:* *Layer 1: <100 µm* *Layer 2: < 200 µm* Grain size: < 100 *µm* Grain shape: *Symplectite: needle-like Spr rods* *Monomineralic layers : granoblastic-polygonal/interlobate* Orientation: *Symplectite Spr vermicules strongly aligned radially w.r.t. layer boundaries*	Equilibrium. Negligible compositional variation described.	500 - 570 °C, 4 - 6 kbar (X_{Al} in Opx; Grt-Crd thermobarometry)	Clockwise decompressive cooling	SSDC	-	-
HM96	Metapelite	Central Zone, Limpopo Belt, Botswana	*Corona 1:* Sil - Opx *Corona 2:* Grt - Qtz	*Corona 1:* *Sil* | Spr+Crd symp | Crd | *Opx* *Corona 2:* *Grt* | Opx+Crd symp | *Qtz*	Corona thickness: *Corona 1: Layer 1: < 80 µm; Layer 2: < 400 µm* *Corona 2: < 500 µm* Vermicule size: *Corona 1: not resolvable* *Corona 2: 50 - 200 µm* Vermicule spacing: *Corona2: ~ 20 µm.* Vermicule Shape: *Symplectite phases: vermicular* *Monomineralic layers: granoblastic-polygonal* Orientation: *Spr rods radially oriented w.r.t. layer boundaries* *Opx vermicules perpendicular to layer boundaries*	No systematic variation recorded for any phases. *Corona 2:* Symplectite Opx: X_{Mg} = 0.68 - 0.75; 4 - 9.0 Al_2O_3 wt% Crd: X_{Mg} = 0.85 - 0.89	~ 800 °C and ~ 6 kbar (Grt-Opx thermometry, FMASH *P,T* grid)	Isothermal uplift followed by isobaric cooling	SSDC	-	-

CJ91: Carlson and Johnson, (1991); CPG89: Clarke et al., (1989); K03: Kelsey et al., (2003b); WPC02: White et al., (2002); KS99: Kriegsman et al., (1999); N02: Norlander et al., (2002); H06: Hollis et al., (2006); G80: Grew, (1980); B04: Baldwin et al., (2004); ACK07: Alvarez-Valero et al., (2007); T06: Tong and Wilson, (2006); G72: Griffin, (1972); MA83: Mongkoltip and Ashworth, (1983); G(88): Grant, (1988); J86: Joesten, (1986); WM73: Whitney and Mclelland, (1973); D89: Droop, (1989); LAL87: Lal et al., (1987); O04: Osanai et al., (2004); T04: Tamashiro et al., (2004); ZH07: Zulbati and Harley, (2007); M98: Markl et al., (1998); BPS97: Baker et al., (1987); BKO03: Brandt et al., (2003); TM85: Tracey and McLellan, (1985); TVR06: Tsunogae and Van Reenen, (2006); HM96: Hisada and Miyano, (1996).

3.6 Conditions of corona formation

Pressure and temperature conditions for corona formation in pelites and mafic rocks are summarized in Figure 3.8. In general, thermobarometric estimates for the average *P-T* conditions of corona formation in mafic and pelitic rocks are above the wet solidus for their respective bulk rock compositions. The few exceptions plotting below the solidus may be attributed to retrograde compositional resetting with cooling. Although the actual solidus for each unique corona bulk composition is not available, Figure 3.8 suggests that corona formation on both the retrograde and prograde paths is likely a suprasolidus process. The final corona layer configuration is that preserved immediately above the solidus for each local corona bulk composition. This is in agreement with phase equilibria modelling of White and Powell (2002), which demonstrated that melt loss is required for the preservation of granulite assemblages and that subsequent reaction is suppressed until the new solidus is crossed at higher temperatures during younger metamorphic events.

Retrograde corona development is constrained to the immediate post-peak, suprasolidus *P-T* path. Since most melt is lost at or near peak conditions (White and Powell, 2002), only a fraction of melt is retained in the restitic post-peak assemblage. Reduced melt volumes with cooling limit length-scales of diffusion to the extent that diffusion-controlled corona growth occurs. On the prograde path, the low melt volumes required for kinetically-constrained corona growth are only commonly realised in mafic rocks, owing to their intrinsic anhydrous bulk composition, and in dry, restitic pelitic compositions that have lost melt in an earlier metamorphic event. White and Powell (2009) distinguish between two types of coronas formed either on the prograde or retrograde paths, i.e., progressive or non-progressive. Progressive coronas develop on the same *P-T* path as the assemblage that they replace, in response to a smooth change in *P-T* conditions from those that produced the peak assemblage (e.g., Johnson et al., 2004; Hollis et al., 2006; Kelsey et al., 2003b). Non-progressive coronas develop in a separate *P-T* event to those that generate the peak assemblage (e.g., Johnson and Carlson, 1990; McFarlane et al., 2003).

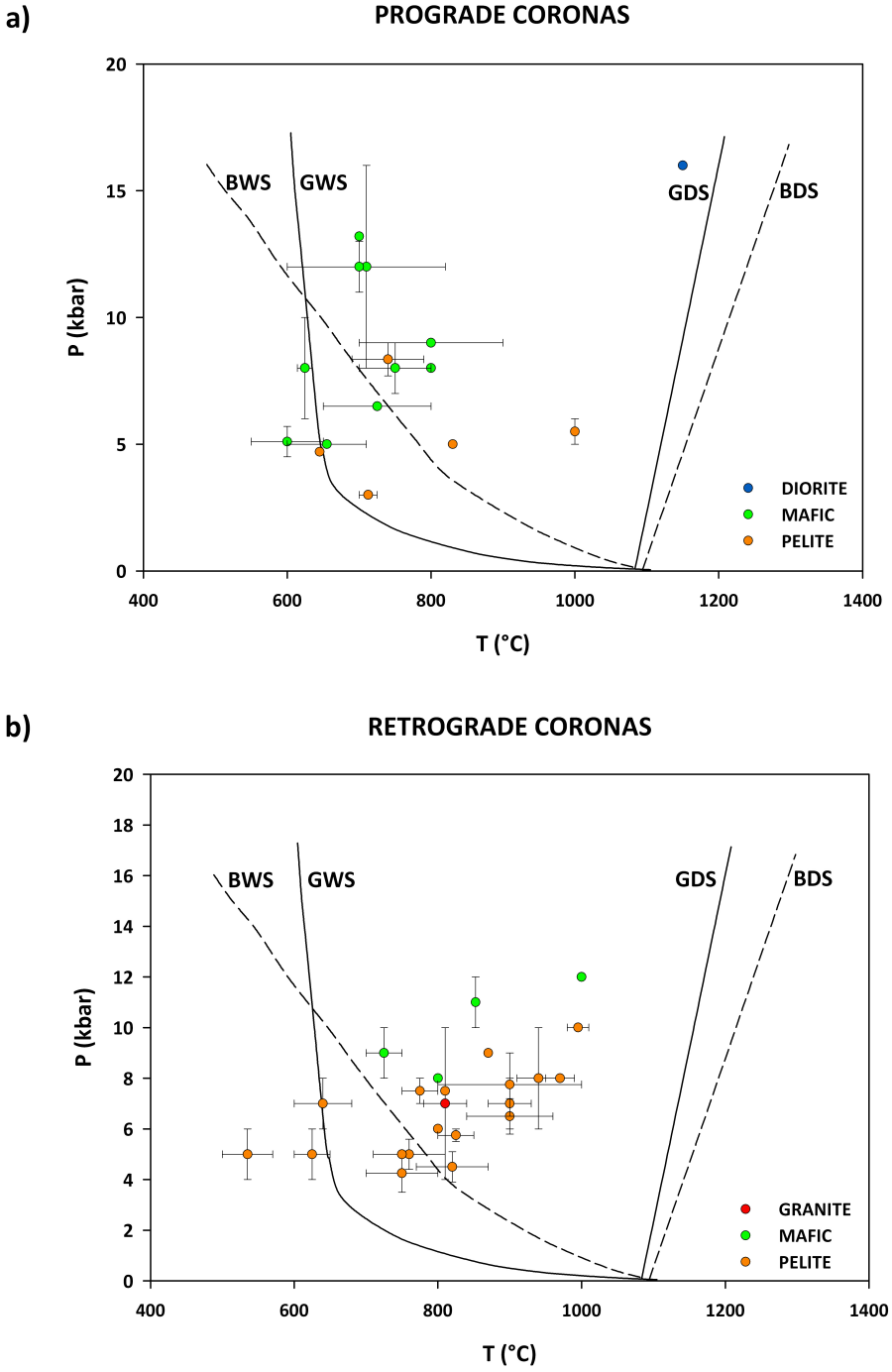

Figure 3.8: Summary of P-T conditions of formation for coronas reviewed in this study. (a) P-T conditions for prograde coronas. (b) P-T conditions for retrograde coronas. In general, conditions of corona formation occur above the wet solidus for each respective bulk composition. The few coronas that plot at lower temperatures than the wet solidi may be subject to retrograde diffusional resetting of the thermometers and, in reality, may have formed at higher suprasolidus temperatures. Error bars are for the range of each estimate. BWS = wet basalt solidus; GWS = wet granite solidus; GDS = dry granite solidus and BDS = Dry basalt solidus. Solidi were digitised in P-T space from geosciences resource database available at http://www.geosci.usyd.edu.au/users/prey/Granite/Granite.html.

3.7 Corona microstructure and compositional zonation

Corona microstructure in prograde and retrograde coronas reviewed in this study is summarized in Figure 3.9. The average maximum corona layer thickness in mafic prograde coronas is 475 µm (range: 70 - 1000 µm, n = 19) and average maximum vermicule size is 118 µm (range: 50 - 300 µm, n = 19). Pelitic prograde coronas are characterized by an average maximum corona thickness of 496 µm (range: 75 - 1500 µm; n = 13) and an average maximum vermicule size of 115 µm (range: 10 - 300 µm, n = 13). Mafic and pelitic prograde coronas do not differ significantly with respect to maximum corona layer thickness and vermicule size. However, pelitic prograde coronas developed in contact metamorphic aureoles appear to exhibit greater maximum corona layer thicknesses compared to regional pelitic prograde coronas (Figure 3.9a).

Most retrograde coronas reviewed in the literature occur in pelitic bulk compositions. Pelitic retrograde coronas are characterized by an average maximum corona thickness of 571 µm (range: 100 - 3000 µm; n = 28) and an average maximum vermicule size of 147 µm (range: 20 - 500 µm, n = 28). The average maximum corona layer thickness in mafic retrograde coronas is 262 µm (range: 80 - 500 µm, n = 5) and average maximum vermicule size is 27 µm (range: 10 - 40 µm, n = 5). Reduced maximum corona thickness and smaller maximum vermicule size in retrograde mafic coronas compared to retrograde pelitic coronas attests to more restricted length-scales of diffusion in melt-poor, anhydrous, mafic bulk rock compositions. Increased maximum layer thickness and vermicule size in prograde mafic coronas compared to retrograde mafic coronas (Figure 3.9) is due to greater length-scales of diffusion in more melt-rich bulk compositions with protracted reaction along the prograde path. Prograde pelitic coronas do not differ significantly from retrograde pelitic coronas with respect to microstructure (Figure 3.9).

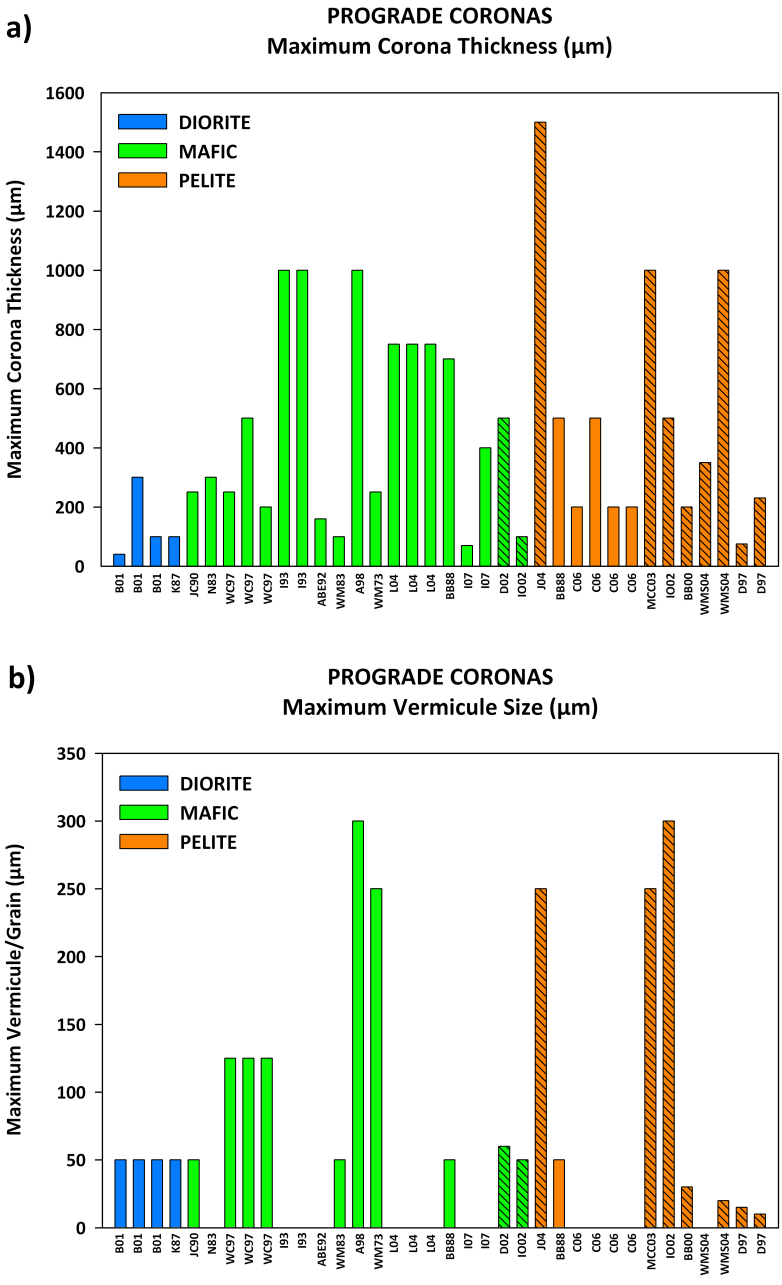

Figure 3.9: Variation in corona microstructure in mafic and pelitic bulk rock compositions. (a) Variation in maximum corona thickness in prograde coronas. (b) Variation in maximum vermicule size in prograde coronas. Hatched bars are prograde coronas from contact aureoles.

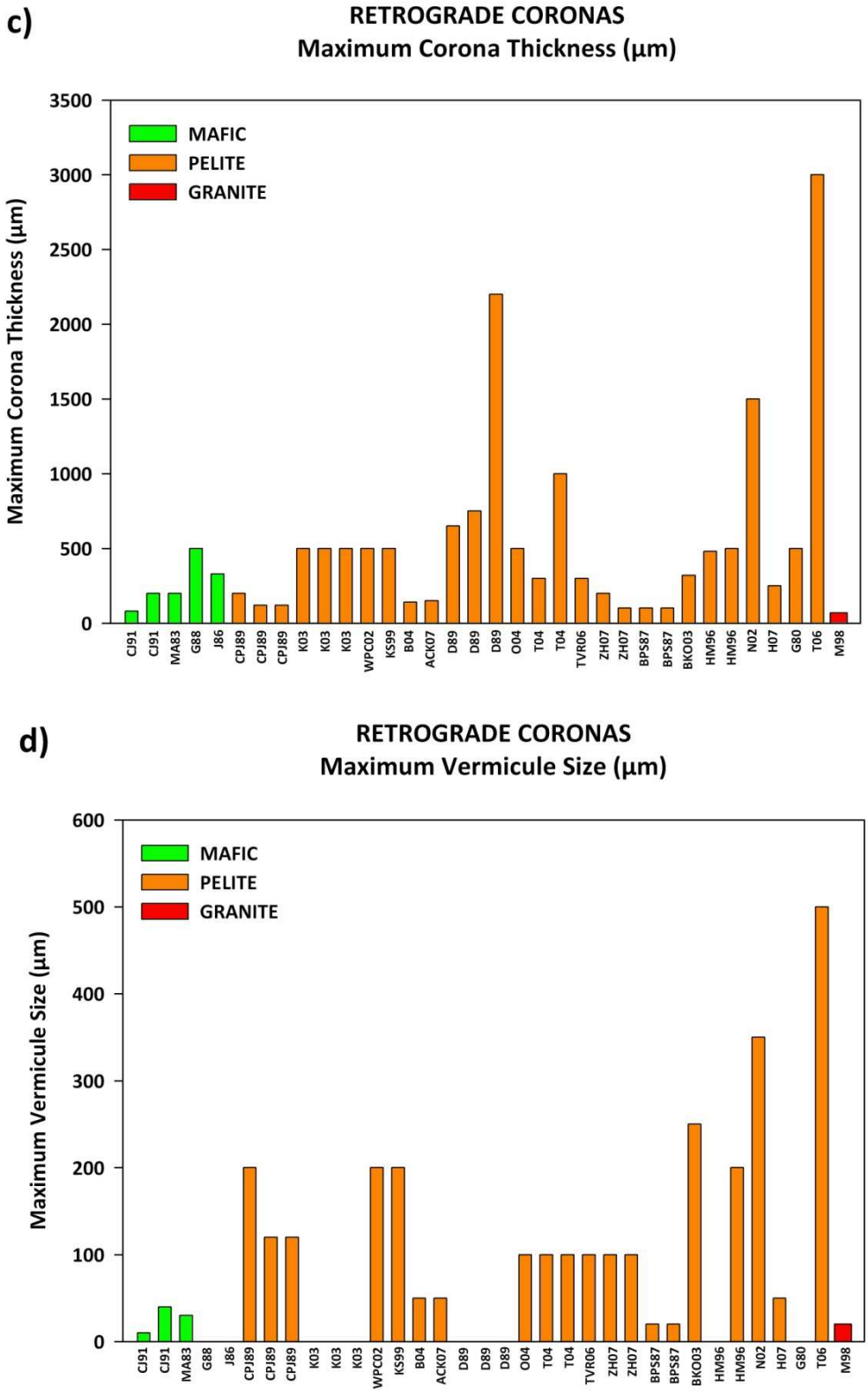

Figure 3.9 continued: Variation in corona microstructure in mafic and pelitic bulk rock compositions. (c) Variation in maximum corona thickness in retrograde coronas. (d) Variation in maximum vermicule size in retrograde coronas.

Complex compositional zonation is commonly observed in coronas (Figure 3.10). Fully equilibrated coronas, where no compositional zonation or chemical potential gradients exist, are rare. In the population of coronas studied, only 30% were fully equilibrated, of which 60% were in pelitic bulk compositions. Commonly, coronas exhibit asymmetric zonation across the band as a whole, reflecting variable length-scales of diffusion for major components during single-stage, steady-state growth (e.g., Ashworth et al., 1998 - A98; Johnson et al., 2004 - J04). Less commonly, radial zonation occurs within a product layer or vermicule from the core to the rim indicative of sequential corona growth (e.g., Zulbati et al., 2007 - ZH07, Figure 3.10). The maximum magnitude of zonation in X_{Mg} of orthopyroxene across a corona band in the coronas reviewed is 0.08 (Kriegsman et al., 1999 - K99; Osanai et al., 2004 - O04; Figure 3.10) and 0.07 in cordierite (Baker et al., 1987 - BKS87; Figure 3.10). Unfortunately, Al content in orthopyroxene is expressed as y(Opx), Al^{IV} and Al wt% in the literature commonly without accompanying raw analyses, so that they cannot be recomputed to a single formulation of Al in orthopyroxene to aid comparison. Maximum asymmetric zonation magnitude with respect to y(Opx) is 0.08 in Hollis et al. (2006) - H06; 0.13 with respect to Al^{IV} (a.p.f.u.) (Brandt et al., 2003 - BKO03) and 0.05 with respect to recalculated molecular proportion (Hisada and Miyano, (1996) - H96). Maximum magnitude of zonation in garnet is 0.22 for X_{Grs} (White and Clarke, 1997 - WC97), 0.18 for X_{Alm} (Indares, 1993 - I93) and 0.17 for X_{Prp} (Koons et al., 1987 - K87). Maximum magnitude in plagioclase zonation ($\Delta X_{An} = 0.42$) across a corona was observed by Baldwin et al. (2004 - B04).

Product phase zonation makes the application of quantitative thermobarometry exceptionally difficult. Asymmetric compositional zonation is consistent with steady-state, diffusion-controlled layer growth and, in this case, local equilibria between mineral pairs in corona layers do not reflect discrete *P-T* conditions but, rather, compositional partitioning of the corona domain during steady-state growth at constant *P* and *T*. Symmetric, radial zoning of phases with respect to grain boundaries is more consistent with a sequential corona formation model, where initially corona layers may develop by steady-state diffusion at (P_1,T_1), equilibrate given sufficient time and then, with subsequent change in *P* and *T*, partially re-equilibrate under new *P-T* conditions (P_2, T_2) reflected in the rim compositions (e.g., White and Clarke, 1997).

In some instances, corona product phases in local equilibrium adjacent to a reactant possess low enough variance to apply a conventional thermobarometer. For example, Baldwin et al. (2004) obtained *P-T* conditions of corona formation from Grt-Opx-Pl-Qtz equilibria using garnet rim and orthopyroxene-plagioclase symplectite compositions in direct contact. Some authors have applied conventional thermobarometers to spatially segregated phases in a corona that are not in direct contact (e.g., Brandt et al., 2003). This approach is only valid if there is no variation in phase composition across the corona band and chemical potentials gradients do not exist.

Ashworth et al. (1998) derived a non-equilibrium extension to conventional thermobarometry based on open-system, steady-state diffusion modelling of coronas that has been successfully employed to estimate *P-T* conditions of formation of asymmetrically-zoned coronas (Ashworth et al., 2001). The principles of non-equilibrium thermobarometry are outlined in Chapter 5 and Appendix A. Unfortunately, non-equilibrium thermobarometry, like conventional thermobarometry, is very sensitive to uncertainties in compositional data and prone to underestimating peak temperatures of formation, because of retrograde resetting upon cooling. The preferred thermobarometric technique for coronas entails phase equilibria modelling in THERMOCALC (e.g., Johnson et al., 2004), where modes and phase compositions are used to jointly constrain a field of equilibration in *P-T-X* space. Information regarding local bulk compositional controls on corona evolution may be gleaned from *T-X* pseudosections. This technique is however, also constrained by the requirement that the corona system is in equilibrium. New functionality in THERMOCALC allows the modelling of corona textures in chemical potential space (White et al., 2008). Observed phase zonation across a corona may now be compared directly with predicted compositions at a range of temperatures and pressures for a corona across which chemical potential gradients prevail.

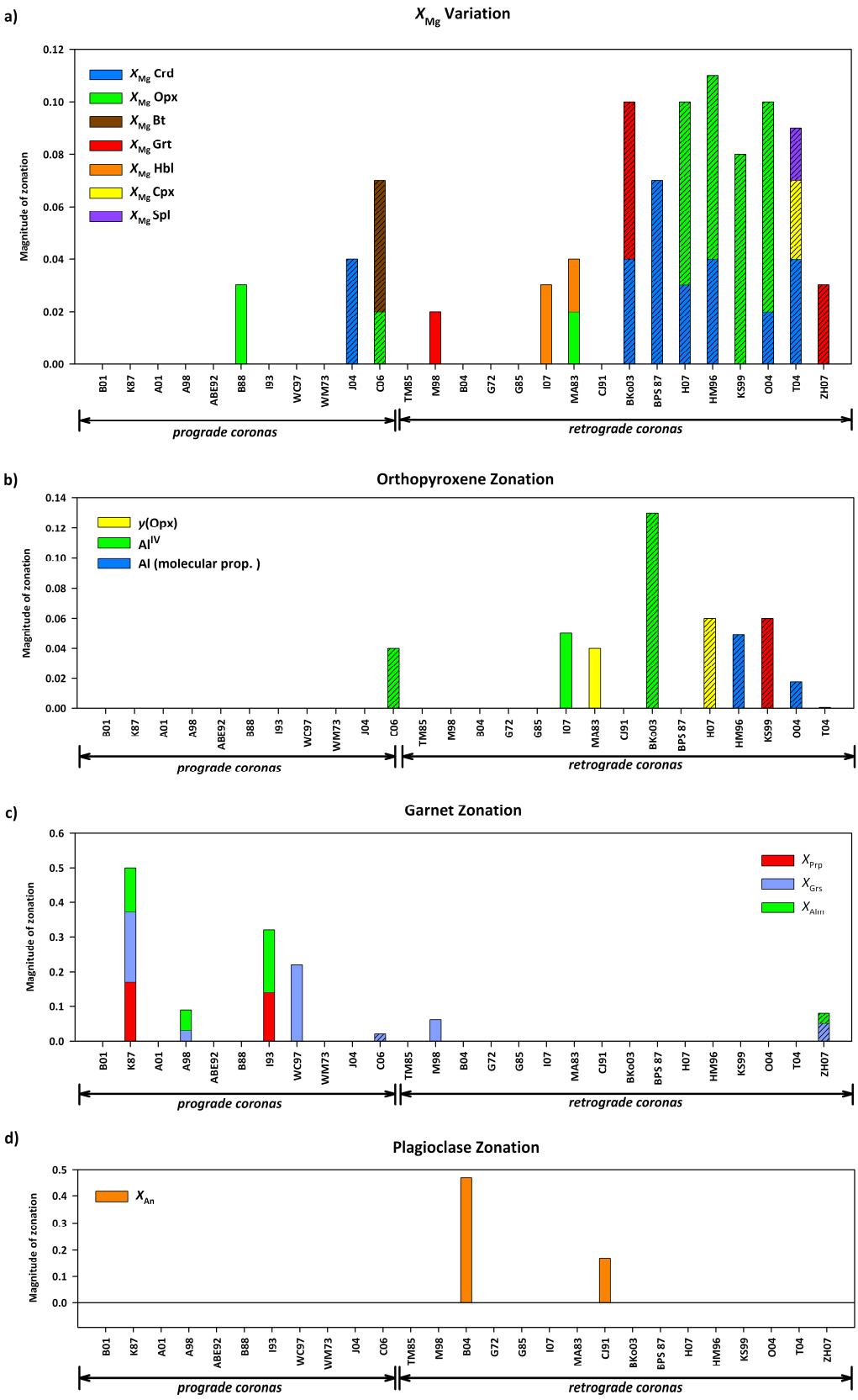

Figure 3.10: Magnitude of compositional zonation in product corona bands. Hatched fields indicate pelitic bulk rock compositions; unhatched are mafic. (a) X_{Mg} variation in product phases. (b) Variation in Al content in orthopyroxene across each corona (c) Garnet zonation across each corona. (d) Plagioclase zonation across coronas where it is documented.

3.8 Quantitative modelling of coronas

Diffusion modeling of metamorphic reactions began in earnest with the foundational work of J.B. Thompson (1959) and Korzhinskii (1959). These workers demonstrated that infinitesimally small regions of rock can attain local equilibrium in the presence of chemical potential gradients for all or some components. This meant that even if the system is in disequilibrium as a whole with gradients in chemical potentials of components in the intergranular medium, it is nevertheless possible to relate the mineral assemblage at any point to the chemical potentials at that point. Korzhinskii (1959) devised a graphical method for plotting a saturation surface in chemical potential space that allowed determination of relative chemical potential differences across a series of layers. This method facilitated an understanding of how layer sequences would evolve as components diffuse down chemical potential gradients. The limitation of Korzhinskii's technique is that many diffusion paths from one reactant to another are possible in the chemical potential diagram, such that more than one possible layer sequence evolves for a particular *P-T* condition (Nishiyama, 1983).

A decade later, the irreversible or, rather, nonequilibrium thermodynamics necessary to rigorously model reaction bands was formulated by Fisher (1973, 1975, 1977). Fisher demonstrated that, in layered reaction products, mineral layers grown by reaction at their contacts and the stoichiometry of the layer contact reactions are determined by the relative diffusion fluxes of components within the layer. Furthermore, component fluxes and chemical potential differences across each layer attain steady-state values as a function of the rate of production and consumption of phases in the layer (Fisher, 1975).

Joesten (1977) combined the approaches of Fisher and Korzhinskii into a hybrid methodology that allowed the prediction of a unique sequence of mineral layers produced by steady-state diffusion for a given choice of phenomenological coefficients in an isochemical system. Joesten's model is based on three fundamental assumptions: first, diffusing components are in local equilibrium with contiguous minerals at every point in a corona, despite the fact that the corona as a whole is in disequilibrium; second, component fluxes and chemical potential gradients remain constant at each point in the corona in a steady-state throughout its

evolution; and third, all components are considered to be conserved within the reaction band, i.e., there is no communication with a system beyond the boundaries of the reaction bands; the system is closed.

Joesten's model required the simultaneous solution of three sets of equations independently relating component fluxes to chemical potential gradients in a layer, chemical potential gradients to each other in the presence of a mineral with a particular composition, and the flux change between layers to reaction coefficients at layer boundaries (Ashworth and Sheplev, 1997). It is possible to evaluate the stability of a multilayer reaction band for a postulated set of intergranular diffusion coefficients if the compositions of the phases in each band are known. The model predicts the relative widths of layers in the reaction band, modal proportions of phases within each layer, component fluxes across layers and reaction stoichiometry at layer boundaries.

Early attempts to model corona textures using Joesten's formalism focussed on corona reaction bands formed between olivine and plagioclase in metagabbros (e.g., Nishiyama, 1983; Joesten, 1986; Grant, 1988). This early work was hindered by the closed system constraint in Joesten's model. For example, Grant (1988) was unable to produce enough Ca from the observed reactant plagioclase to accommodate all the Ca in the corona reaction band. Furthermore, the failure of Joesten's model to account for hydrous corona products, such as hornblende, from anhydrous plagioclase and olivine reactants, led workers to embrace an open-system, metasomatic, modification to Joesten's model. An open-system modification was introduced by Johnson and Carlson (1990) and Ashworth and Birdi (1990). Material balance calculations allowed them to determine the external component fluxes across the outer boundaries of the corona, thereby accommodating open-system communication with the enclosing matrix. Johnson and Carlson (1990) and Carlson and Johnson (1991) introduced external boundary flux equations to model open-system behaviour. Ashworth and Birdi (1990) treated metasomatic fluxes at corona boundaries as theoretical 'phases' with 'negative' compositions where components were lost from the system and 'positive' compositions where they entered into the corona system. The open system studies of Johnson and Carlson (1990) and Carlson and Johnson (1991) also indicated that corona growth may not occur as a 'single-

stage, steady-state process', but rather through a number of 'transient states', reflecting gradual changes in the composition of the reactants and external fluxes throughout corona evolution, thus manifesting as variable product assemblages (Figure 3.6a).

Open-system diffusion models for coronas had much more success in explaining corona development in a variety of different bulk compositions, from mafic rocks to metapelites, than the earlier isochemical models (Johnson and Carlson, 1990; Carlson and Johnson, 1991; Ashworth and Birdi, 1990; Ashworth et al., 1992; Ashworth, 1993; Ashworth and Sheplev, 1997; Ashworth et al., 1998). Ashworth (1993) noted that, although the overall extent of reaction was constrained by highly mobile components with large diffusive fluxes, the actual spatial arrangement of minerals in coronas appears to be strongly controlled by those components with lower diffusivities, particularly Al and Si. He noted that, in all cases, an Al-rich layer (commonly symplectitic) was located adjacent to the most aluminous reactant, grading into an Al-poor layer adjacent to the less aluminous reactant, and both separated by a 'transitional' layer of intermediate contents of Al. A schematic corona demonstrating his observations is included in Figure 3.11.

Ashworth and Birdi (1990) compared the Al/Si ratio in aluminous reactants and the adjacent symplectite for a number of coronas using an isocon diagram (Figure 3.12; Grant, 1986). The isocon plot suggested that total Al and Si (strictly $A1O_{3/2}$ and SiO_2, since the components used are oxides following Fisher, 1973) included within the phases in the symplectite appear to be 'inherited stoichiometrically' from the adjacent reactant. Any mismatch between Al/Si ratio of the reactant and individual phases comprising the symplectite is accommodated by proportional growth of symplectite phases in the appropriate ratio such that cumulatively the Al/Si ratio is retained. Ashworth and Birdi (1990) proposed that this was a consequence of low diffusivities of Al and Si relative to, inter alia, Fe, Mg and Ca. According to them, any disagreement between the Al/Si ratio of the symplectite and reactant implies open-system behaviour for these components. The endmember scenario involving near-complete open-system behaviour for Al and Si would, thus, be a monomineralic reaction band in which mismatch in Al/Si ratio is greatest. Mongkoltip and Ashworth (1983) ventured still further that the occurrence of two

immobile diffusing components is a necessary condition for symplectite formation. This assertion agreed with the metasomatic equilibrium theory of Korzhinskii (1965), which states that any divariant equilibrium assemblage of *n* phases contains at least *n* inert or immobile components. Assessing open- or closed-sytem behaviour for Al and Si is critical in deciding which assumptions are realistic when determining the overall reaction. If Al and Si are preserved in the symplectite, then closure to Al and Si can be used to constrain the system such that it is not underdetermined. If this assumption is not valid, constant volume may have to be assumed (Carlson and Johnson, 1991).

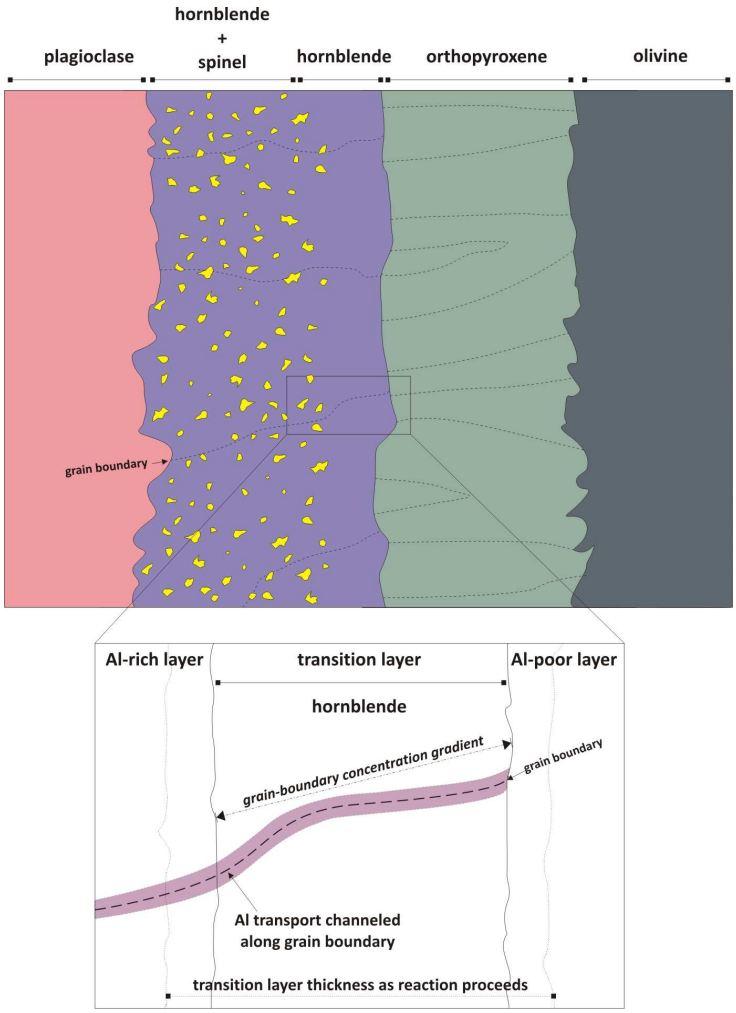

Figure 3.11: Sketch of a typical corona developed between plagioclase and olivine in metagabbros (after Ashworth, 1993). As reaction proceeds, layers grow by diffusion along grain boundaries of requisite components down concentration gradients to layer boundaries where they are consumed in the production of product phases. Al is considered to be the most immobile diffusing species, since Al concentration gradients are most marked. Al exerts the greatest control on segregation of corona products in bands, from the most Al-rich symplectite adjacent to plagioclase to Al-poor orthopyroxene adjacent to olivine.

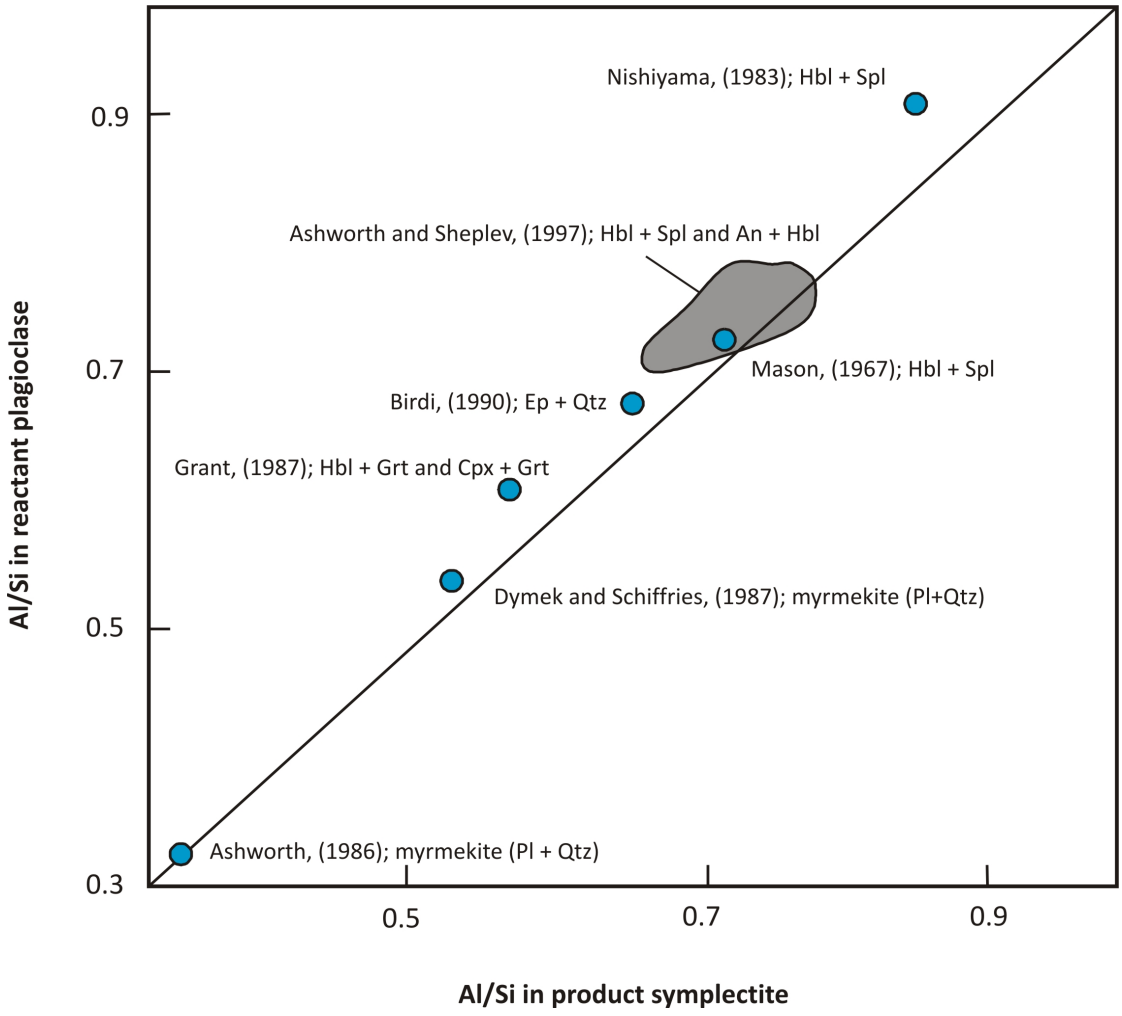

Figure 3.12: Isocon plot of Al/Si ratios in symplectites and the adjacent reactant plagioclase. The isocon line represents Al/Si ratios that are preserved exactly between reactant and products. Any deviation from this line indicates a degree of open-system behaviour. In general, analysed symplectites from the literature plot above the isocon line, suggesting that the Al/Si ratio is lower in the product symplectite than it is in the reactant plagioclase, i.e., the corona system is losing Al to the external system relative to Si or gaining Si relative to Al with prolonged reaction.

The first thermodynamic treatment of conservation of volume during diffusion metasomatism was undertaken by Carmichael (1987). Carmichael challenged the assumption that pressure remains constant during irreversible diffusion metasomatism. During reaction, there is a tendency for the boundary between two juxtaposed reactants to be displaced perpendicular to the interface between the reactants at a magnitude corresponding to the change of volume of solid phases of the reaction. If there is any mechanical resistance to this displacement, constant

volume replacement is approached. Carmichael (1987) was able to model a field of nonhydrostatic stress induced by migration of the boundary between reactants. The stress field is oriented in a manner which opposes the displacement and strain accompanying the migration of the boundary. The stress field may be dissipated by either rock deformation or secondary mass transfer out of the reacting volume. According to Carmichael's model, the secondary mass transfer may be so efficient as to eliminate the induced stress caused by boundary migration, such that the original interface between reactants remains undisplaced. This realization allows us to make reasonable approximations for the original boundary between reactants (and the relative proportions of reactants involved in reaction) such that an overall reaction may be derived.

The spacing of lamellae or vermicules in symplectites reflects a balance between diffusive energy dissipation and grain boundary energy. Ashworth and Chambers (2000) derived a theory quantifying this relationship employing both non-equilibrium thermodynamics and the principle of maximum rate of energy dissipation. Accordingly, the spacing of lamellae in a symplectite for a particular reaction is a function of the reaction rate (i.e., reaction front velocity), diffusion coefficient of the slowest-diffusing components and the width of the reaction front:

$$\lambda = \sqrt[3]{\frac{L\delta}{v}}$$

λ = lamellae spacing; L = Onsager diffusion coefficient

δ = reaction front width; v = reaction rate

The finest symplectitic intergrowths are predicted to occur when reaction rates greatly exceed diffusion coefficients for the slowest-diffusing species for a particular reaction front width.

Despite advances in diffusion metasomatic modelling of coronas in the early 1990's, success was still limited in that commonly more than one stable layer sequence was computable for the same inputs. Sheplev et al. (1991, 1992a, b) presented a criterion to determine which non-unique solution is more thermodynamically stable compared to others and, thus, is the correct solution. The criterion was formalized by Ashworth

and Sheplev (1997), and extended so as to obtain a measure of the affinity of reaction or, rather, departure from equilibrium, preserved in the corona. A final refinement to the open-system diffusion model for coronas was derived by Ashworth et al. (2001), in which ratios of the affinity of independent endmember reactions modelled for a corona are compared to ratios calculated from an internally-consistent thermodynamic database (Holland and Powell, 1998; upgrade November 2003). The pressure and temperature where the ratio of model endmember reaction affinities and real endmember reaction affinities approach the same value is considered to represent the closure pressure and temperature below which the corona remained inert to reaction. For the first time, quantitative estimates of pressure and temperature of formation of minerals in disequilibrium is facilitated through this method.

Advances in phase equilibria modelling allow geologically realistic corona compositional systems to be modelled in *P-T-X* (Johnson et al., 2004) and chemical potential space (White et al., 2008; White and Powell, 2009). It is possible to predictively model corona evolution with changing effective bulk composition through progressive metasomatic exchange of components with the external matrix in a rock and/or partitioning of the corona effective bulk composition with reduced length-scales of component diffusion on cooling (e.g., Johnson et al., 2004; White et al., 2008). White et al. (2008) demonstrated how quantitative modelling of chemical potential gradients in a corona allows the measured compositions to be related to modelled chemical potential relationships and the amount of each component that has to be transported in or out of a particular volume of rock to equalise chemical potentials. These authors stress that the concept of a 'static' effective bulk composition may be suitable for modelling the peak metamorphism of a rock, but potentially misleading when modelling the evolution of complex corona textures in which the bulk composition of the corona changes with time, either owing to external flux into the corona or varying length-scales of diffusion. Cogniscance of this fact must be taken when modelling coronas with conventional *P-T* pseudosections in which effective bulk compositions are assumed constant during reaction (e.g., Johnson et al., 2004; White et al., 2008; White and Powell, 2009).

3.9 Discussion

In this chapter, mechanisms of corona formation have been reviewed, i.e., single-stage, steady-state, diffusion-controlled vs. sequential corona development. It is critical to determine which model of corona formation is applicable if the correct information from a corona is to be derived when constructing the *P*-*T* path for a terrane. Asymmetric zonation in phase composition across a corona band is the most rigorous indication of single-stage, steady-state, diffusion-controlled corona growth.

A comprehensive review of prograde and retrograde coronas for mafic and pelitic bulk rock compositions from both regional and contact aureole terranes has been undertaken in this study. Major controls on corona mineralogy include: *P*, *T* and aH_2O during formation (Section 3.5.1); mechanism of formation (Section 3.5.2); reactant bulk compositions and extent of metasomatic exchange with the surrounding rock (Section 3.5.3); relative diffusion rates for major components (Section 3.5.4) and associated deformation and strain (Section 3.5.5). In general, corona formation appears to be a suprasolidus process (Section 3.6), requiring the presence of melt or fluid for reaction to occur (Figure 3.8). With respect to corona microstructure, prograde coronas developed in contact metamorphic aureoles exhibit greater maximum corona thickness (Figure 3.9a) than in regional coronas for pelitic rocks. Mafic and pelitic prograde coronas do not differ significantly with respect to maximum corona layer thickness and vermicule size. Reduced maximum corona thickness and smaller maximum vermicule size (Figure 3.9c, d) in retrograde mafic coronas compared to retrograde pelitic coronas attests to more restricted length-scales of diffusion in melt-poor, anhydrous, mafic bulk rock compositions. Increased maximum layer thickness and vermicule size in prograde mafic coronas compared to retrograde mafic coronas (Figure 3.9) is due to greater length-scales of diffusion in potentially more melt-rich bulk compositions with protracted reaction along the prograde path. Prograde pelitic coronas do not differ significantly from retrograde pelitic coronas with respect to microstructure (Figure 3.9).

High variance local equilibria in a corona and disequilibrium across the corona as a whole, preclude the application of conventional thermobarometry when determining *P, T* conditions of corona formation. Although tempting, the asymmetric zonation in phase composition across a corona, indicative of single-stage, steady-state, diffusion

controlled formation, should not be interpreted as a record of discrete *P-T* conditions during successive layer growth along the *P-T* path. Rather, the local equilibria between mineral pairs in corona layers reflect compositional partitioning of the corona domain during steady-state growth at constant *P* and *T*. A non-equilibrium extension of conventional thermobarometry derived by Ashworth et al. (2001) should be used with phase equilibria modelling in THERMOCALC to constrain *P-T* evolution of coronas.

Open-system, metasomatic diffusion modelling of coronas that form during single-stage, steady-state, diffusion-controlled reaction allows the affinity of corona reaction to be determined and the degree of disequilibrium to be quantitatively assessed (Section 3.8). This information coupled with phase equilibria modelling of the corona domain (e.g., Johnson et al., 2004) reveals information about corona reaction mechanisms and controls on equilibration extent. In Chapter 4, the Vredefort coronas are described petrographically and compared with those reviewed in Chapter 3, to establish both their uniqueness and potential to preserve information related to controls on corona growth and equilibration in general, typically obscured in coronas from more common settings. Diffusion modelling on the Vredefort coronas is then undertaken in Chapter 5 and complemented with phase equilibria modelling of corona domains in Chapter 6.